J. Plasma Phys. (2025), *vol*. 91, E23
Published by Cambridge University Press

doi:10.1017/S0022377824001673

Application of quadruple Beltrami state on Saturnian dusty plasma

S.M. Gondal †

Department of Physics, University of Engineering and Technology, Lahore 54890, Pakistan

(Received 11 June 2024; revised 7 December 2024; accepted 10 December 2024)

This investigation explores the potential formation of a relaxed equilibrium state, specifically the quadruple Beltrami state, in a three-component dusty plasma consisting of electrons, ions and negatively charged dust particles. This equilibrium state is derived by employing momentum-balanced equations along with Ampere's law. The quadruple Beltrami state is a composite of four Beltrami states, each associated with four distinct eigenvalues. Using the variational principle, we obtained the same relaxed state based on the system's constraints, which include magnetofluid energy, and the helicity of electrons, ions and dust particles. The unified flow is also derived. Dynamo action is investigated in two configurations: a rectangular geometry and a rectangular geometry with an internal conductor. Small-scale turbulent dynamo behaviour is observed in the former, while large-scale turbulent dynamo effects are noted in the latter. The magnitude of the magnetic field is found to be greater in the configuration with an internal conductor. Additionally, flow profiles are plotted as functions of Beltrami parameters and density variations of plasma species. This study contributes to the understanding of relaxation theory and the underlying physics of systems with an internal conductor, such as Saturn (planetary rings around a magnetosphere) and Jupiter magnetosphere, Uranus, Neptune, etc.

Key words: plasma dynamics, astrophysical plasmas, plasma confinement

1. Introduction

The relaxed structures epitomize a self-organized phenomenon in plasma termed the Beltrami state. This state, characterized by its force-free nature, signifies that the system's current density ($\nabla \times \boldsymbol{B} = \boldsymbol{J}$) aligns parallel to its magnetic field $\boldsymbol{B}$ (Shivamoggi 2011), expressed as

$$\boldsymbol{J} = \lambda \boldsymbol{B}, \tag{1.1}$$

where λ is a constant (Woltjer 1958). It encompasses diverse structural forms like twisted, helical and spiral configurations observed across different systems. The Beltrami field arises in various plasma models like the reversed field pinch (Ogawa 2002) and field reversal configurations (Sun *et al.* 2017). Vortex formations like hurricanes (Nebbat & Annou 2010) serve as illustrations of the Beltrami state within Earth's atmosphere. It represents a divergence-free vector field (Yoshida & Giga 1990) governing incompressible flows. Taylor's relaxation model (Taylor 1974, 1986) elucidates this phenomenon within

† Email address for correspondence: sabagondal@uet.edu.pk

single-fluid plasma systems, known as magnetohydrodynamics (MHD). It posits that the rate of energy decay surpasses that of helicity, symbolizing the structural complexity of the magnetic field within the system. The Beltrami field aids in elucidating the traits observed in solar coronal structures (Gold & Hoyle 1958), with analogous structures found in various astrophysical entities. These include twisted flux tubes, which have been extensively researched. Additionally, the storage of magnetic energy via helical winding (Salingaros 1990) in toroidal configurations has been explored within the context of force-free fields. However, the single Beltrami field falls short in explaining the relaxed structures observed in tokamaks.

In the study of multi-species plasmas, it has been observed that the vorticity associated with each fluid imposes constraints (Avinash 1991, 1992) on the system, indicating a non-force-free relaxed state. For systems consisting of two fluids, such as electrons and ions, a relaxation theory proposed by Steinhauer & Ishida (1998) describes energy minimization while maintaining helicity constraints. This theory predicts the emergence of pressure and strong flow, phenomena absent in single-fluid plasmas.

In the context of Hall magnetohydrodynamic (HMHD) plasmas, Mahajan & Yoshida (1998) and Yoshida & Mahajan (1999) introduced a relaxation theory known as the double Beltrami state. A new framework based on variational principles (Yoshida & Mahajan 2002) was also presented, considering three invariants: energy, magnetic helicity and generalized helicity involving vorticity. In discussions related to two-fluid plasmas (Yoshida *et al.* 2001) and multi-fluid plasmas (Mahajan & Yoshida 2000; Yoshida *et al.* 2001; Guzdar, Mahajan & Yoshida 2005), there has been a focus on high-confinement boundary layers, which are associated with increased pressure within the plasma system.

The relaxation theory was extended to higher-order Beltrami states, including the triple Beltrami state (Bhattacharyya, Janaki & Dasgupta 2003; Gondal & Iqbal 2021*a*) and then the quadruple Beltrami state (Shatashvili, Mahajan & Berezhiani 2016), through the use of a multi-fluid plasma system (Gondal *et al.* 2017; Gondal & Iqbal 2020*a*; Gondal 2020*b*; Gondal & Iqbal 2020*c*). The triple Beltrami state is composed of three individual Beltrami states, each with its own scale parameter, while the quadruple Beltrami state is formed from four distinct Beltrami states, each with its own scale parameter.

Mathematical models have been developed to explain catastrophic transformations, showing how the double Beltrami state transitions into single Beltrami states in two-fluid (Ohsaki *et al.* 2001, 2002) and three-fluid plasma systems (Gondal *et al.* 2019). Additionally, the double Beltrami state has been applied to model solar eruptions (Kagan & Mahajan 2010). The Beltrami flow has been used to investigate phenomena such as spinning black holes (Bhattacharjee & Feng 2020*a*) and accretion disks (Bhattacharjee & Stark 2020*b*). Similarly, the mathematical model of the quadruple Beltrami state in a slab geometry has been applied to elucidate the formation of relaxed structures in the Earth's mesosphere (Gondal 2020*b*).

In this current research, our objective is to investigate the relaxed structures within Saturn's atmosphere using the mathematical model of the quadruple Beltrami state in a coplanar rectangular geometry. This geometry mirrors the dual configuration of Saturn's magnetosphere and its rings.

The dual configuration elucidates the role of an internal conductor within a plasma system. The presence of an internal conductor coil introduces an innovative approach to relaxation theory, particularly under conditions of high pressure and flow. Experimental investigations into the presence of an internal conductor in a plasma system have been conducted through various means, such as confining turbulent plasmas using internal coils (Yoshida *et al.* 2004) or linear mirror devices (Valanju, Mahajan & Quevedo 2006), and studying the impact of biased electrodes (Saitoh *et al.* 2004*a*, *b*). Yoshida *et al.*

https://doi.org/10.1017/S0022377824001673 Published online by Cambridge University Press

(1998) examined plasma confinement using the internal coil device, while in cylindrical configurations (Yoshida *et al.* 1999), solutions for the single-Beltrami-state case have been observed. The magnetic confinement of several devices employing internal coils (Yoshida *et al.* 2007) has been studied both theoretically (Yoshida *et al.* 1999; Nakashima *et al.* 2002; Gondal & Iqbal 2021*b*; Gondal 2022) and experimentally (Saitoh *et al.* 2004*c*).

Our study also delves into the dynamo mechanics present in both geometries. We consider a system consisting of three fluids: electrons, ions and negatively charged dust particles. The behaviour of the magnetic and flow fields under different conditions suggests distinct dynamo mechanisms at play. In the present work, it is observed, in a simple rectangular geometry (Saturn's magnetosphere), where the magnetic field is weaker than the flow field, the dynamics align with a fast dynamo process. In such a regime, where fluid motions are dominant, rapid stretching and folding of magnetic field lines can efficiently amplify the field, a characteristic feature of fast dynamos. In contrast, rectangular geometry with an internal conductor (Saturn's E ring) presents a scenario where the magnetic field is stronger than the flow field. This configuration supports a slow dynamo, where the stronger magnetic field constrains the fluid motions, leading to a more organized interaction and slower amplification of the magnetic field. The presence of an internal conductor in the ring further enhances the magnetic field strength compared with the simpler rectangular geometry of the magnetosphere. The investigation aims to explore the characteristics of both the composite flow and the individual fluids within the system. Additionally, this exploration involves varying the Beltrami parameters and the concentration of the plasma species. To elucidate the dynamo mechanics and the influence of plasma species velocities within the Saturn atmosphere, all graphs are plotted using plasma parameters derived from real Saturnian plasma (Shohaib *et al.* 2022; Wahlund *et al.* 2009). This work may also prove beneficial in studying and comprehending the physics of planets with dual configurations, such as Jupiter (Yoshida *et al.* 2004), Neptune, Pluto, near-Earth plasma sheet (Wang, Cao & Liu 2016), ionosphere (Wahlund *et al.* 1998; Mahmood & Ur-Rehman 2013) etc. Additionally, it may offer insights into explaining nuclear fusion devices featuring an internal conductor.

The manuscript is structured as follows.

I. Introduction: we outline the problem.
II. Basic equations: we present a set of equations to elucidate the dynamics of plasma species.
III. Formalism: the formalism of the relaxed equilibrium system is discussed.
IV. Flows: we discuss the unified flow and the flows of individual components of plasma species.
V. Constraints: we elaborate on the constraints of the system and the presentation of the generalized Bernoulli conditions
VI. Solutions: two sets of solutions for the relaxed quadruple Beltrami state are derived.
VII. Results: we display the magnetic and flow profiles of the vortex pattern based on Beltrami parameters and the impact of plasma species density variation.
VIII. Conclusion: we conclude the work.

2. Basic equations

We investigate the relaxed structures within a collisionless dusty plasma, taking into account three plasma species: electrons (s_e), ions (s_i) and negatively charged dust particles (s_d). Additionally, Z_{s_d} denotes the charge state of the negatively charged dust particles, while the ions are assumed to be singly ionized. It is presumed that the plasma equilibrium

https://doi.org/10.1017/S0022377824001673 Published online by Cambridge University Press

condition is fulfilled, which can be expressed as

$$Z_{s_d} n_{s_d} + n_{s_e} = n_{s_i}, \tag{2.1}$$

here, n_{s_e}, n_{s_i} and n_{s_d} are the symbols to represent the equilibrium densities of the components: electrons, ions and dust particles, respectively. The masses assigned to the plasma constituents, encompassing electrons, ions and dust particles, are designated as m_{s_e}, m_{s_i} and m_{s_d}, respectively. The normalized system of governing fluid equations, designed to elucidate the dynamics of the relaxed equilibrium structures, is presented as follows:

$$\frac{\partial}{\partial t}\left(\boldsymbol{U}_{s_e} - \boldsymbol{A}\right) + \nabla \psi_{s_e} - \boldsymbol{U}_{s_e} \times \left(\nabla \times \boldsymbol{U}_{s_e} - \boldsymbol{H}\right) = 0, \tag{2.2}$$

$$\frac{\partial}{\partial t}\left(\boldsymbol{U}_{s_i} + M_{s_i}\boldsymbol{A}\right) + \nabla \psi_{s_i} - \boldsymbol{U}_{s_i} \times \left(\nabla \times \boldsymbol{U}_{s_i} + M_{s_i}\boldsymbol{H}\right) = 0, \tag{2.3}$$

$$\frac{\partial}{\partial t}\left(\boldsymbol{U}_{s_d} - Z_{s_d} M_{s_d}\boldsymbol{A}\right) + \nabla \psi_{s_d} - \boldsymbol{U}_{s_d} \times \left(\nabla \times \boldsymbol{U}_{s_d} - Z_{s_d} M_{s_d}\boldsymbol{H}\right) = 0, \tag{2.4}$$

where $\psi_{s_e} = -\phi + p_{s_e} + U_{s_e}^2/2$, $\psi_{s_i} = M_{s_i}\phi + (M_{s_i}/N_{s_i})p_{s_i} + U_{s_i}^2/2$ and $\psi_{s_e} = -Z_{s_d}M_{s_d}\phi + (M_{s_d}/N_{s_d})p_{s_d} + U_{s_d}^2/2$, while the mass ratios of the plasma components are $M_{s_d} = m_{s_e}/m_{s_d}$ and $M_{s_i} = m_{s_e}/m_{s_i}$. In the given context, $\boldsymbol{U}_j$ $(j = s_e, s_i, s_d)$ represent the electrons, ions and dust particles velocities, respectively, normalized by the Alfvén velocity $V_A = B_0/\sqrt{\mu_0 n_{s_e} m_{s_e}}$ (B_0 is the arbitrary value of magnetic field and μ_0 represents the permeability of free space). The pressure p_j is scaled by B_0^2/μ_0. The electric field $\boldsymbol{E}$ can be described as follows:

$$\boldsymbol{E} = -\nabla\phi - \frac{\partial \boldsymbol{A}}{\partial t}. \tag{2.5}$$

The vector potential $\boldsymbol{A}$ which can be defined as $\boldsymbol{H} = \nabla \times \boldsymbol{A}$, where $\boldsymbol{H}$ is the magnetic field and the electrostatic scalar potential ϕ are normalized by $\lambda_{s_e} B_0$ and $\lambda_{s_e} B_0 V_A$, respectively. The units of time and space are in terms of electron plasma period (inverse of electron gyrofrequency ω_p^{-1}) and electron skin depth λ_{s_e} (Iqbal & Shukla 2012), where $\omega_p^{-1} = V_A/\lambda_{s_e}$ and $\lambda_{s_e} = V_A/\omega_p = \sqrt{m_{s_e}/\mu_0 n_{s_e} e^2}$. The plasma frequency (Miyamoto 1980) corresponding to ω_p is expressed as eB_0/m_{s_e}, where e is the charge with a value of 1.6×10^{-19} C. It is important to note that the effects of dust charge fluctuations, acting as a source of dissipation and contributing to the formation of shock structures, are not the primary focus of our present consideration. Upon using the curl operator on the dynamic equations presented in (2.2)–(2.4), we derive the subsequent set of vortex dynamic equations:

$$\frac{\partial}{\partial t}\left(\nabla \times \boldsymbol{U}_{s_e} - \boldsymbol{H}\right) - \nabla \times \left\{\boldsymbol{U}_{s_e} \times \left(\nabla \times \boldsymbol{U}_{s_e} - \boldsymbol{H}\right)\right\} = 0, \tag{2.6}$$

$$\frac{\partial}{\partial t}\left(\nabla \times \boldsymbol{U}_{s_i} + M_{s_i}\boldsymbol{H}\right) - \nabla \times \left\{\boldsymbol{U}_{s_i} \times \left(\nabla \times \boldsymbol{U}_{s_i} + M_{s_i}\boldsymbol{H}\right)\right\} = 0, \tag{2.7}$$

$$\frac{\partial}{\partial t}\left(\nabla \times \boldsymbol{U}_{s_d} - Z_{s_d} M_{s_d}\boldsymbol{H}\right) - \nabla \times \left\{\boldsymbol{U}_{s_d} \times \left(\nabla \times \boldsymbol{U}_{s_d} - Z_{s_d} M_{s_d}\boldsymbol{H}\right)\right\} = 0, \tag{2.8}$$

and we ultimately reach the following equation:

$$\frac{\partial \boldsymbol{\Omega}_j}{\partial t} - \nabla \times [\boldsymbol{V}_j \times \boldsymbol{\Omega}_j] = 0, \tag{2.9}$$

which represents the compact form of (2.6)–(2.8). In this context, $\boldsymbol{\Omega}_j (j = s_e, s_i, s_d)$, ($\boldsymbol{\Omega}_{s_e} = \nabla \times \boldsymbol{U}_{s_e} - \boldsymbol{H}$, $\boldsymbol{\Omega}_{s_i} = \nabla \times \boldsymbol{U}_{s_i} + M_{s_i}\boldsymbol{H}$ and $\boldsymbol{\Omega}_{s_d} = \nabla \times \boldsymbol{U}_{s_d} - Z_{s_d}M_{s_d}\boldsymbol{H}$) denote the

https://doi.org/10.1017/S0022377824001673 Published online by Cambridge University Press

generalized vorticities, and $\boldsymbol{V}_j$

$$\boldsymbol{V}_j = \boldsymbol{U}_j, \tag{2.10}$$

represents the velocities of the plasma components. To complete the system, Ampere's law (Mahajan & Yoshida 1998; Mahajan & Lingam 2020; Shatashvili *et al.* 2016; Gondal *et al.* 2017; Gondal & Iqbal 2020*a*; Gondal 2020*b*; Gondal & Iqbal 2020*c*) is applied, yielding the subsequent expression:

$$\boldsymbol{U}_{s_i} = \frac{\mathbf{1}}{N_{s_i}} \left(\boldsymbol{\nabla} \times \boldsymbol{H} + \boldsymbol{U}_{s_e} + Z_{s_d} N_{s_d} \boldsymbol{U}_{s_d} \right), \tag{2.11}$$

where the symbols N_{s_i} and N_{s_d} are defined as $N_{s_i} = n_{s_i}/n_{s_e}$ and $N_{s_d} = n_{s_d}/n_{s_e}$, the ratio of the ions to electrons and dust particles to electrons, respectively.

3. Relaxed Beltrami equation in a dusty plasmas

By adhering to the Mahajan–Shatashvili (Shatashvili *et al.* 2016) methodology, we derive the Beltrami condition, which is the steady-state condition of (2.9),

$$\Lambda_j \boldsymbol{\Omega}_j = \boldsymbol{U}_j. \tag{3.1}$$

Expressed in terms of the plasma components – electrons, ions and dust particles – the equilibrium Beltrami condition can be characterized as

$$a_{s_e} \boldsymbol{U}_{s_e} = \boldsymbol{\nabla} \times \boldsymbol{U}_{s_e} - \boldsymbol{H}, \tag{3.2}$$

$$a_{s_i} \boldsymbol{U}_{s_i} = \boldsymbol{\nabla} \times \boldsymbol{U}_{s_i} + M_{s_i} \boldsymbol{H}, \tag{3.3}$$

$$a_{s_d} \boldsymbol{U}_{s_d} = \boldsymbol{\nabla} \times \boldsymbol{U}_{s_d} - Z_{s_d} M_{s_d} \boldsymbol{H}, \tag{3.4}$$

where the symbols a_{s_e}, a_{s_i} and a_{s_d} represent the vorticity to the flow ratio of the plasma particles – electrons, ions and dust particles, respectively. The inverse of these symbols are also termed as Beltrami parameters ($\Lambda_j = 1/a_j$, where $j = s_e$, s_i and s_d) (Gondal *et al.* 2017). Obtaining the flow of electrons $\boldsymbol{U}_{s_e}$ is achieved by inserting (2.11) into (3.3),

$$\boldsymbol{U}_{s_e} = K_1 \left(\boldsymbol{\nabla} \times \right)^2 \boldsymbol{H} - K_2 \boldsymbol{\nabla} \times \boldsymbol{H} + K_3 \boldsymbol{H} + K_4 \boldsymbol{U}_{s_d}, \tag{3.5}$$

where $K_1 = (a_{s_i} - a_{s_e})^{-1}$, $K_2 = a_{s_i}/K_1$, $K_3 = (1 + N_{s_i} M_{s_i} + Z_{s_d}^2 N_{s_d} M_{s_d})/K_1$ and $K_4 = Z_{s_d} N_{s_d} (a_{s_d} - a_{s_i})/K_1$. Substituting the value of $\boldsymbol{U}_{s_e}$ from (3.5) into (3.2) provides the expression for the flow of dust particles, which can be expressed as

$$\boldsymbol{U}_{s_d} = l_1 \left(\boldsymbol{\nabla} \times \right)^3 \boldsymbol{H} - l_2 \left(\boldsymbol{\nabla} \times \right)^2 \boldsymbol{H} + l_3 \boldsymbol{\nabla} \times \boldsymbol{H} - l_4 \boldsymbol{H}, \tag{3.6}$$

where $l_1 = [Z_{s_d} N_{s_d} (a_{s_e} - a_{s_d})(a_{s_d} - a_{s_i})]^{-1}$, $l_2 = (a_{s_e} + a_{s_i})/l_1$, $l_3 = (a_{s_e} a_{s_i} + 1 + N_{s_i} M_{s_i} + Z_{s_d}^2 N_{s_d} M_{s_d})/l_1$ and $l_4 = (a_{s_i} + (a_{s_e} + a_{s_i} - a_{s_d}) Z_{s_d}^2 N_{s_d} M_{s_d} + a_{s_e} N_{s_i} M_{s_i})/l_1$. Employing the aforementioned (3.6) into (3.4) ultimately yields the relaxed equilibrium state, recognized

https://doi.org/10.1017/S0022377824001673 Published online by Cambridge University Press

as the quadruple relaxed Beltrami state,

$$(\nabla\times)^4\boldsymbol{H} - b_1(\nabla\times)^3\boldsymbol{H} + b_2(\nabla\times)^2\boldsymbol{H} + b_3\nabla\times\boldsymbol{H} + b_4\boldsymbol{H} = 0, \tag{3.7}$$

where

$$b_1 = a_{s_e} + a_{s_i} + a_{s_d}, \tag{3.8}$$

$$b_2 = a_{s_e}a_{s_i} + a_{s_i}a_{s_d} + a_{s_d}a_{s_e} + 1 + N_{s_i}M_{s_i} + Z_{s_d}^2N_{s_d}M_{s_d}, \tag{3.9}$$

$$b_3 = N_{s_i}M_{s_i}\left(a_{s_d} + a_{s_e}\right) + Z_{s_d}^2N_{s_d}M_{s_d}\left(a_{s_e} + a_{s_i}\right) + \left(a_{s_i} + a_{s_d}\right) + a_{s_e}a_{s_i}a_{s_d}, \tag{3.10}$$

$$b_4 = N_{s_i}M_{s_i}a_{s_d}a_{s_e} + Z_{s_d}^2N_{s_d}M_{s_d}a_{s_e}a_{s_i} + a_{s_i}a_{s_d}. \tag{3.11}$$

The equilibrium state, as indicated by (3.7), in a three-component dusty plasma is a composite of four distinct single equilibrium Beltrami states. The overall solution of (3.7) can be characterized in terms of the following eigen expression (Shatashvili, Mahajan & Berezhiani 2019):

$$\nabla\times\boldsymbol{B}_\delta = \lambda_\delta\boldsymbol{B}_\delta, \tag{3.12}$$

where the eigenfunction is $\boldsymbol{B}_\delta$ and the eigenvalue is λ_δ. Here, $\delta = 1, 2, 3, 4$ describes four states having four individual eigenvalues. Equation (3.12) can also be interpreted as

$$(\mathrm{curl} - \lambda_1)(\mathrm{curl} - \lambda_2)(\mathrm{curl} - \lambda_3)(\mathrm{curl} - \lambda_4)\boldsymbol{H} = 0, \tag{3.13}$$

by expressing the operator $(\nabla\times)$ as 'curl'. In the above expression, $\boldsymbol{H} = \boldsymbol{H}_1 + \boldsymbol{H}_2 + \boldsymbol{H}_3 + \boldsymbol{H}_4$ and λ_1, λ_2, λ_3 and λ_4 represent the four distinct eigenvalues. Solving (3.13) yields the same fourth-order equation as previously derived in (3.7),

$$(\nabla\times)^4\boldsymbol{H} - b_1(\nabla\times)^3\boldsymbol{H} + b_2(\nabla\times)^2\boldsymbol{H} + b_3\nabla\times\boldsymbol{H} + b_4\boldsymbol{H} = 0, \tag{3.14}$$

in the above expression, b_1, b_2, b_3 and b_4 are the constants, which can be read as in terms of eigenvalues,

$$b_1 = \lambda_1 + \lambda_2 + \lambda_3 + \lambda_4, \tag{3.15}$$

$$b_2 = \lambda_1\lambda_2 + \lambda_2\lambda_3 + \lambda_3\lambda_4 + \lambda_4\lambda_1 + \lambda_1\lambda_3 + \lambda_2\lambda_4, \tag{3.16}$$

$$b_3 = \lambda_1\lambda_2\lambda_3 + \lambda_2\lambda_3\lambda_4 + \lambda_3\lambda_4\lambda_1 + \lambda_4\lambda_1\lambda_2, \tag{3.17}$$

$$b_4 = \lambda_1\lambda_2\lambda_3\lambda_4. \tag{3.18}$$

The values of λ_1, λ_2, λ_3 and λ_4 (Gondal *et al.* 2017; Gondal & Iqbal 2020*a*; Gondal 2020*b*; Gondal & Iqbal 2020*c*) can be determined as $\lambda_1 = (b_1 + 2r + 2\delta)/4$, $\lambda_2 = (b_1 + 2r - 2\delta)/4$, $\lambda_3 = (b_1 - 2r + 2\delta)/4$ and $\lambda_4 = (b_1 - 2r - 2\delta)/4$, where $r = (\sqrt{b_1^2 - 4b_2 + 4Y})/2$, $Y = (d - 3u^2 + 3u\alpha_1)/3u$, $u = \sqrt[3]{(q/2) + \sqrt{(q/2)^2 + (d/3)^3}}$, $q = (9\alpha_1\alpha_2 - 2\alpha_1^3 - 27\alpha_3)/27$, $d = (3\alpha_2 - \alpha_1^2)/3$, $\alpha_1 = b_2$, $\alpha_2 = b_3b_1 - 4b_4$ and $\alpha_3 = b_3^2 +$

https://doi.org/10.1017/S0022377824001673 Published online by Cambridge University Press

$b_1^2 b_4 - 4 b_2 b_4$. For $r \neq 0$, δ and ξ are given as

$$\left.\begin{aligned} \delta &= \sqrt{\frac{3}{4} b_1^2 - r^2 - 2 b_2 + \frac{1}{4r}(4 b_1 b_2 - 8 b_3 - b_1^3)}, \\ \xi &= \sqrt{\frac{3}{4} b_1^2 - r^2 - 2 b_2 - \frac{1}{4r}(4 b_1 b_2 - 8 b_3 - b_1^3)}, \end{aligned}\right\} \tag{3.19}$$

while for $r = 0$, δ and ξ read as

$$\left.\begin{aligned} \delta &= \sqrt{\tfrac{3}{4} b_1^2 - 2 b_2 + 2\sqrt{Y^2 - 4 b_4}}, \\ \xi &= \sqrt{\tfrac{3}{4} b_1^2 - 2 b_2 - 2\sqrt{Y^2 - 4 b_4}}. \end{aligned}\right\} \tag{3.20}$$

The discourse presented in the above equations highlights that the eigenvalues are contingent on Beltrami parameters, plasma particle densities, the mass of plasma particles and the charge state of dust particles. These eigenvalues may exhibit either a real nature or a combination of real and a pair of complex conjugates. Therefore, by manipulating the Beltrami parameters and plasma parameters, we have the ability to alter the characteristics of the eigenvalues and subsequently influence the nature of the relaxed structures. In § 7, we delved into the analysis of velocity profiles by varying the Beltrami parameters and the densities of plasma species.

4. Unified flow

To determine the unified flow $\boldsymbol{U}$, we can employ the following momentum equation:

$$\boldsymbol{U} = \frac{\rho_{s_e} \boldsymbol{U}_{s_e} + \rho_{s_i} \boldsymbol{U}_{s_i} + \rho_{s_d} \boldsymbol{U}_{s_d}}{\rho}, \tag{4.1}$$

where ρ is the mass density of the system which can be described as $\rho = \rho_{s_e} + \rho_{s_i} + \rho_{s_d}$. Here, ρ_{s_e}, ρ_{s_i} and ρ_{s_d} represent the density of electrons, ions and negatively charged dust fluids, respectively ($\rho_{s_e} = n_{s_e} m_{s_e}$, $\rho_{s_i} = n_{s_i} m_{s_i}$ and $\rho_{s_d} = n_{s_d} m_{s_d}$). By substituting the flow of ions from (2.11) into the aforementioned (4.1), we obtain

$$\boldsymbol{U} = c_1 \boldsymbol{\nabla} \times \boldsymbol{H} + c_2 \boldsymbol{U}_{s_e} + c_3 \boldsymbol{U}_{s_d}, \tag{4.2}$$

where $c_1 = \rho_{s_i}/\rho N_{s_i}$, $c_2 = (\rho_{s_e} + \rho_{s_i}/N_{s_i})/\rho$ and $c_3 = (\rho_{s_d} + \rho_{s_i} Z_{s_d} N_{s_d}/N_{s_i})/\rho$. By inserting the value of the electron flow $\boldsymbol{U}_{s_e}$ into the equation above, we obtain

$$\boldsymbol{U} = d_1 (\boldsymbol{\nabla}\times)^2 \boldsymbol{H} - d_2 \boldsymbol{\nabla} \times \boldsymbol{H} + d_3 \boldsymbol{H} + d_4 \boldsymbol{U}_{s_d}, \tag{4.3}$$

where $d_1 = c_2 K_1$, $d_2 = c_2 K_2 - c_1$, $d_3 = c_2 K_3$ and $d_4 = c_2 K_4 + c_3$. Now, by incorporating the value of the flow of negatively charged dust particles $\boldsymbol{U}_{s_d}$ from (3.6) into the above equation, we arrive at the ultimate expression for the unified flow, which can be read as

$$\boldsymbol{U} = e_1 (\boldsymbol{\nabla}\times)^3 \boldsymbol{H} - e_2 (\boldsymbol{\nabla}\times)^2 \boldsymbol{H} + e_3 \boldsymbol{\nabla} \times \boldsymbol{H} - e_4 \boldsymbol{H}, \tag{4.4}$$

where $e_1 = d_4 l_1$, $e_2 = d_4 l_2 - d_1$, $e_3 = d_4 l_3 - d_2$ and $e_4 = d_4 l_4 - d_3$.

https://doi.org/10.1017/S0022377824001673 Published online by Cambridge University Press

5. Physical invariants and the equilibrium state

In the realm of plasma dynamics, Mahajan's exploration of systems involving S fluids reveals the existence of $S+1$ invariants (Mahajan 2008; Mahajan & Lingam 2015). In the current research, the system under investigation features three distinctive components: electrons, ions and negatively charged dust particles. Consequently, the constraints for this tripartite plasma system encompass magnetofluid energy (E), the generalized helicity of electrons (h_{s_e}), the generalized helicity of ions (h_{s_i}) and the generalized helicity of negatively charged dust grains (h_{s_d}). By employing (2.6)–(2.8), these four integral invariants can be elegantly expressed as

$$E = \frac{1}{2}\left(\boldsymbol{U}_{s_e}^2 + \frac{N_{s_i}}{M_{s_i}}\boldsymbol{U}_{s_i}^2 + \frac{N_{s_d}}{Z_{s_d}M_{s_d}}\boldsymbol{U}_{s_d}^2 + \boldsymbol{H}^2\right), \tag{5.1}$$

$$h_{s_e} = \frac{1}{2}\int_v \left(\boldsymbol{U}_{s_e} - \boldsymbol{A}\right)\cdot\left(\boldsymbol{\nabla}\times\boldsymbol{U}_{s_e} - \boldsymbol{H}\right)\mathrm{d}v, \tag{5.2}$$

$$h_{s_i} = \frac{1}{2}\int_v \left(\boldsymbol{U}_{s_i} + M_{s_i}\boldsymbol{A}\right)\cdot\left(\boldsymbol{\nabla}\times\boldsymbol{U}_{s_i} + M_{s_i}\boldsymbol{H}\right)\mathrm{d}v, \tag{5.3}$$

$$h_{s_d} = \frac{1}{2}\int_v \left(\boldsymbol{U}_{s_d} - Z_{s_d}M_{s_d}\boldsymbol{A}\right)\cdot\left(\boldsymbol{\nabla}\times\boldsymbol{U}_{s_d} - Z_{s_d}M_{s_d}\boldsymbol{H}\right)\mathrm{d}v. \tag{5.4}$$

Another approach, termed the variational principle (Sudan 1979; Steinhauer & Ishida 1997; Mahajan & Yoshida 1998), can also be employed to recover the relaxed magnetized equilibrium state,

$$\delta\left(E - \mu_{s_e}h_{s_e} - \mu_{s_i}h_{s_i} - \mu_{s_d}h_{s_d}\right) = 0, \tag{5.5}$$

where the symbols μ_{s_e}, μ_{s_i} and μ_{s_d} represent the Lagrangian multipliers. By solving the aforementioned equations concurrently and treating $\delta\boldsymbol{A}$, $\delta\boldsymbol{U}_{s_i}$ and $\delta\boldsymbol{U}_{s_i}$, as independent parameters, we derive

$$\frac{1}{a_{s_e}}\left(\boldsymbol{H} - \boldsymbol{\nabla}\times\boldsymbol{U}_{s_e}\right) + \frac{N_{s_i}}{a_{s_i}}\left(M_{s_i}\boldsymbol{H} + \boldsymbol{\nabla}\times\boldsymbol{U}_{s_i}\right) + \frac{N_{s_d}}{a_{s_d}}\left(Z_{s_d}M_{s_d}\boldsymbol{H} + \boldsymbol{\nabla}\times\boldsymbol{U}_{s_d}\right) = \boldsymbol{\nabla}\times\boldsymbol{H}, \tag{5.6}$$

$$a_{s_i}\boldsymbol{U}_{s_i} = \boldsymbol{\nabla}\times\boldsymbol{U}_{s_i} + M_i\boldsymbol{H}, \tag{5.7}$$

$$a_{s_d}\boldsymbol{U}_{s_d} = \boldsymbol{\nabla}\times\boldsymbol{U}_{s_d} + Z_{s_d}M_{s_d}\boldsymbol{H}, \tag{5.8}$$

considering $\mu_e = -1/a_{s_e}$, $\mu_{s_i} = N_{s_i}/a_{s_i}M_{s_i}$ and $\mu_{s_d} = -N_{s_d}/a_{s_d}M_{s_d}Z_{s_d}$. Inserting (5.7)–(5.8) into (5.6), the resulting expression is

$$\boldsymbol{U}_{s_i} = \frac{1}{N_{s_i}}\left(\boldsymbol{\nabla}\times\boldsymbol{H} + Z_{s_i}M_{s_i}\boldsymbol{U}_{s_i} + \boldsymbol{U}_{s_i}\right). \tag{5.9}$$

It has been noted that the set of equations (5.7)–(5.9) obtained through the variational principle bears resemblance to our earlier set of equilibrium equations (3.2)–(3.4). This observation indicates that the self-organization of ordered structures can be discerned through the variational principle.

The Beltrami alignment illustrated in (2.4)–(2.3) imposes the subsequent generalized Bernoulli conditions, by replacing (2.6)–(2.8) into (2.2)–(2.4), which represent the

https://doi.org/10.1017/S0022377824001673 Published online by Cambridge University Press

macroscopic evolution equations of the plasma species, and setting the time derivative $\partial/\partial t$ equal to 0 (indicating a steady state), we derive the subsequent equations:

$$\nabla\left(\frac{1}{2}U_{s_e}^2 + p_{s_e} - \phi\right) = 0, \tag{5.10}$$

$$\nabla\left(\frac{1}{2}U_{s_i}^2 + \frac{M_{s_i}}{N_{s_i}}p_{s_i} + M_{s_i}\phi\right) = 0, \tag{5.11}$$

$$\nabla\left(\frac{1}{2}U_{s_d}^2 + \frac{M_{s_d}}{N_{s_d}}p_{s_d} - Z_{s_d}M_{s_d}\phi\right) = 0, \tag{5.12}$$

which articulate the equilibrium of all remaining potential forces. Upon integration of the aforementioned set of equations, we obtain

$$f_{s_e} = \tfrac{1}{2}U_{s_e}^2 + p_{s_e} - \phi, \tag{5.13}$$

$$f_{s_i} = \frac{1}{2}U_{s_i}^2 + \frac{M_{s_i}}{N_{s_i}}p_{s_i} + M_{s_i}\phi, \tag{5.14}$$

$$f_{s_d} = \frac{1}{2}U_{s_d}^2 + \frac{M_{s_d}}{N_{s_d}}p_{s_d} - Z_{s_d}M_{s_d}\phi, \tag{5.15}$$

where the constants of integration are f_{s_e}, f_{s_i} and f_{s_d}. The consolidated form of these equations can be described as

$$Constant = P + \tfrac{1}{2}\left(U_{s_e}^2 + U_{s_i}^2 + U_{s_d}^2\right) - \left(1 - M_{s_i} + M_{s_d}\right)\phi, \tag{5.16}$$

where $P = p_{s_e} + M_{s_i}p_{s_i}N_{s_i}^{-1} + Z_{s_d}M_{s_d}p_{s_d}N_{s_d}^{-1}$.

6. Solutions of the field equation

Expressed as the linear sum of four Beltrami states, the quadruple Beltrami field (3.7) can be written as

$$\boldsymbol{H} = C_1\boldsymbol{H}_1 + C_2\boldsymbol{H}_2 + C_3\boldsymbol{H}_3 + C_4\boldsymbol{H}_4. \tag{6.1}$$

In this context, the symbol C_1, C_2,C_3 and C_4 signify the amplitude four Beltrami states. Equation (3.7) denotes a partial differential equation, with ABC flow (Arnold & Khesin 1998) being one of the solutions corresponding to the Beltrami state in the slab geometry. Subsequent to the ABC flow, the derivations for solving (3.7)) are conducted for two distinct modes: (i) a simple rectangular geometry (Gondal *et al.* 2017; Gondal & Iqbal 2020*a*,*c*); and (ii) a coplanar rectangular geometry, which involves a rectangular conducting chamber within the Cartesian coordinate system.

6.1. *Solution of quadruple Beltrami state in a simple rectangular geometry*

Expressing the solution of (3.7) in terms of x, y and z, we get

$$\begin{pmatrix} H_x \\ H_y \\ H_z \end{pmatrix} = \begin{pmatrix} 0 \\ C_1\sin(\lambda_1 x) + C_2\sin(\lambda_2 x) + C_3\sin(\lambda_3 x) + C_4\sin(\lambda_4 x) \\ C_1\cos(\lambda_1 x) + C_2\cos(\lambda_2 x) + C_3\cos(\lambda_3 x) + C_4\cos(\lambda_4 x) \end{pmatrix}, \tag{6.2}$$

where the symbols C_α ($\alpha = 1, 2, 3$ and 4) signify the amplitude. The values of these constants can be determined by applying the following set of boundary conditions:

https://doi.org/10.1017/S0022377824001673 Published online by Cambridge University Press

$|H_y|_{x=X} = g_1$, $|H_z|_{x=0} = g_2$, $|(\nabla \times \boldsymbol{H})_y|_{x=X} = g_3$ and $|(\nabla \times \boldsymbol{H})_z|_{x=0} = g_4$ in (6.2), we obtain

$$g_1 = C_1 \sin(\lambda_1 X) + C_2 \sin(\lambda_2 X) + C_3 \sin(\lambda_3 X) + C_4 \sin(\lambda_4 X), \tag{6.3}$$

$$g_2 = C_1 + C_2 + C_3 + C_4, \tag{6.4}$$

$$g_3 = C_1\lambda_1 \sin(\lambda_1 X) + C_2\lambda_2 \sin(\lambda_2 X) + C_3\lambda_3 \sin(\lambda_3 X) + C_4\lambda_4 \sin(\lambda_4 X), \tag{6.5}$$

$$g_4 = C_1\lambda_1 + C_2\lambda_2 + C_3\lambda_3 + C_4\lambda_4. \tag{6.6}$$

Solving the above equations, we obtain

$$C_1 = \frac{L_1}{L_5}, \quad C_2 = \frac{L_2}{L_5}, \quad C_3 = \frac{L_3}{L_5}, \quad C_4 = \frac{L_4}{L_5}, \tag{6.7a–d}$$

where

$$\begin{aligned} L_1 = {} & [\sin(\lambda_3 X)\sin(\lambda_4 X)(g_4 - g_2\lambda_2) + \sin(\lambda_2 X)(g_3 - g_1\lambda_2)](\lambda_3 - \lambda_4) \\ & + [\sin(\lambda_3 X)\sin(\lambda_2 X)(g_4 - g_2\lambda_4) + \sin(\lambda_4 X)(g_3 - g_1\lambda_4)](\lambda_2 - \lambda_3) \\ & + [\sin(\lambda_2 X)\sin(\lambda_4 X)(g_4 - g_2\lambda_3) + \sin(\lambda_3 X)(g_3 - g_1\lambda_3)](\lambda_4 - \lambda_2), \end{aligned} \tag{6.8}$$

$$\begin{aligned} L_2 = {} & [\sin(\lambda_3 X)\sin(\lambda_1 X)(g_4 - g_2\lambda_4) + \sin(\lambda_4 X)(g_3 - g_1\lambda_4)](\lambda_3 - \lambda_1) \\ & + [\sin(\lambda_3 X)\sin(\lambda_4 X)(g_4 - g_2\lambda_1) + \sin(\lambda_1 X)(g_3 - g_1\lambda_1)](\lambda_4 - \lambda_3) \\ & + [\sin(\lambda_1 X)\sin(\lambda_4 X)(g_4 - g_2\lambda_3) + \sin(\lambda_3 X)(g_3 - g_1\lambda_3)](\lambda_1 - \lambda_4), \end{aligned} \tag{6.9}$$

$$\begin{aligned} L_3 = {} & [\sin(\lambda_1 X)\sin(\lambda_4 X)(g_4 - g_2\lambda_2) + \sin(\lambda_2 X)(g_3 - g_1\lambda_2)](\lambda_4 - \lambda_1) \\ & + [\sin(\lambda_1 X)\sin(\lambda_2 X)(g_4 - g_2\lambda_4) + \sin(\lambda_4 X)(g_3 - g_1\lambda_4)](\lambda_1 - \lambda_2) \\ & + [\sin(\lambda_2 X)\sin(\lambda_4 X)(g_4 - g_2\lambda_1) + \sin(\lambda_1 X)(g_3 - g_1\lambda_1)](\lambda_2 - \lambda_4), \end{aligned} \tag{6.10}$$

$$\begin{aligned} L_4 = {} & [\sin(\lambda_3 X)\sin(\lambda_1 X)(g_4 - g_2\lambda_2) + \sin(\lambda_2 X)(g_3 - g_1\lambda_2)](\lambda_1 - \lambda_3) \\ & + [\sin(\lambda_1 X)\sin(\lambda_2 X)(g_4 - g_2\lambda_3) + \sin(\lambda_3 X)(g_3 - g_1\lambda_3)](\lambda_2 - \lambda_1) \\ & + [\sin(\lambda_2 X)\sin(\lambda_3 X)(g_4 - g_2\lambda_1) + \sin(\lambda_1 X)(g_3 - g_1\lambda_1)](\lambda_3 - \lambda_2), \end{aligned} \tag{6.11}$$

$$\begin{aligned} L_5 = {} & (\lambda_4 - \lambda_1)[\sin(\lambda_4 X)\sin(\lambda_1 X) + \sin(\lambda_3 X)\sin(\lambda_2 X)](\lambda_3 - \lambda_2) \\ & + (\lambda_4 - \lambda_3)[\sin(\lambda_4 X)\sin(\lambda_3 X) + \sin(\lambda_2 X)\sin(\lambda_1 X)](\lambda_2 - \lambda_1) \\ & + (\lambda_2 - \lambda_4)[\sin(\lambda_2 X)\sin(\lambda_4 X) + \sin(\lambda_3 X)\sin(\lambda_1 X)](\lambda_3 - \lambda_1). \end{aligned} \tag{6.12}$$

6.2. *Solution of quadruple Beltrami state in a rectangular geometry with an internal conductor*

An internal conductor geometry involves embedding a rectangular chamber within another rectangular configuration. Let us assume the length of this submerged rectangular chamber is denoted as x_0 along the x-axis. The solution for (3.7) within this specific region can be expressed as follows:

$$\begin{pmatrix} H_x \\ H_y \\ H_z \end{pmatrix} = \begin{pmatrix} 0 \\ M_1 \sin(\lambda_1 x) + N_1 \cos(\lambda_1 x) + M_2 \sin(\lambda_2 x) + N_2 \cos(\lambda_2 x) \\ M_1 \cos(\lambda_1 x) - N_1 \sin(\lambda_1 x) + M_2 \cos(\lambda_2 x) - N_2 \sin(\lambda_2 x) \end{pmatrix} + \begin{pmatrix} 0 \\ M_3 \sin(\lambda_3 x) + N_3 \cos(\lambda_3 x) + M_4 \sin(\lambda_4 x) + N_4 \cos(\lambda_4 x) \\ M_3 \cos(\lambda_3 x) - N_3 \sin(\lambda_3 x) + M_4 \cos(\lambda_4 x) - N_4 \sin(\lambda_4 x) \end{pmatrix}. \tag{6.13}$$

https://doi.org/10.1017/S0022377824001673 Published online by Cambridge University Press

In this context, the symbols M_α ($\alpha = 1, 2, 3$ and 4) and N_α ($\alpha = 1, 2, 3$ and 4) signify the amplitude. Upon applying the relevant boundary conditions, namely $|B_y|_{x=x_0} = w_1$, $|B_z|_{x=x_0} = w_2$, $|(\nabla \times \boldsymbol{B})_y|_{x=x_0} = w_3$, $|(\nabla \times \boldsymbol{B})_z|_{x=x_0} = w_4$, $|((\nabla\times)^2\boldsymbol{B})_y|_{x=x_0} = w_5$, $|((\nabla\times)^2\boldsymbol{B})_z|_{x=x_0} = w_6$, $|((\nabla\times)^3\boldsymbol{B})_y|_{x=x_0} = w_7$ and $|((\nabla\times)^3\boldsymbol{B})_z|_{x=x_0} = w_8$, we derive the following system of equations:

$$\begin{aligned}
w_1 &= M_1 \sin(\lambda_1 x_0) + N_1 \cos(\lambda_1 x_0) + M_2 \sin(\lambda_2 x_0) + N_2 \cos(\lambda_2 x_0) \\
&\quad + M_3 \sin(\lambda_3 x_0) + N_3 \cos(\lambda_3 x_0) + M_4 \sin(\lambda_4 x_0) + N_4 \cos(\lambda_4 x_0), \qquad (6.14)\\
w_2 &= M_1 \cos(\lambda_1 x_0) - N_1 \sin(\lambda_1 x_0) + M_2 \cos(\lambda_2 x_0) - N_2 \sin(\lambda_2 x_0) \\
&\quad + M_3 \cos(\lambda_3 x_0) - N_3 \sin(\lambda_3 x_0) + M_4 \cos(\lambda_4 x_0) - N_4 \sin(\lambda_4 x_0), \qquad (6.15)\\
w_3 &= \lambda_1 M_1 \sin(\lambda_1 x_0) + \lambda_1 N_1 \cos(\lambda_1 x_0) + \lambda_2 M_2 \sin(\lambda_2 x_0) + \lambda_2 N_2 \cos(\lambda_2 x_0) \\
&\quad + \lambda_3 M_3 \sin(\lambda_3 x_0) + \lambda_3 N_3 \cos(\lambda_3 x_0) + \lambda_4 M_4 \sin(\lambda_4 x_0) + \lambda_4 N_4 \cos(\lambda_4 x_0), \qquad (6.16)\\
w_4 &= \lambda_1 M_1 \cos(\lambda_1 x_0) - \lambda_1 N_1 \sin(\lambda_1 x_0) + \lambda_2 M_2 \cos(\lambda_2 x_0) - \lambda_2 N_2 \sin(\lambda_2 x_0) \\
&\quad + \lambda_3 M_3 \cos(\lambda_3 x_0) - \lambda_3 N_3 \sin(\lambda_3 x_0) + \lambda_4 M_4 \cos(\lambda_4 x_0) - \lambda_4 N_4 \sin(\lambda_4 x_0), \qquad (6.17)\\
w_5 &= \lambda_1^2 M_1 \sin(\lambda_1 x_0) + \lambda_1^2 N_1 \cos(\lambda_1 x_0) + \lambda_2^2 M_2 \sin(\lambda_2 x_0) + \lambda_2^2 N_2 \cos(\lambda_2 x_0) \\
&\quad + \lambda_3^2 M_3 \sin(\lambda_3 x_0) + \lambda_3^2 N_3 \cos(\lambda_3 x_0) + \lambda_4^2 M_4 \sin(\lambda_4 x_0) + \lambda_4^2 N_4 \cos(\lambda_4 x_0), \qquad (6.18)\\
w_6 &= \lambda_1^2 M_1 \cos(\lambda_1 x_0) - \lambda_1^2 N_1 \sin(\lambda_1 x_0) + \lambda_2^2 M_2 \cos(\lambda_2 x_0) - \lambda_2^2 N_2 \sin(\lambda_2 x_0) \\
&\quad + \lambda_3^2 M_3 \cos(\lambda_3 x_0) - \lambda_3^2 N_3 \sin(\lambda_3 x_0) + \lambda_4^2 M_4 \cos(\lambda_4 x_0) - \lambda_4^2 N_4 \sin(\lambda_4 x_0), \qquad (6.19)\\
w_7 &= \lambda_1^3 M_1 \sin(\lambda_1 x_0) + \lambda_1^3 N_1 \cos(\lambda_1 x_0) + \lambda_2^3 M_2 \sin(\lambda_2 x_0) + \lambda_2^3 N_2 \cos(\lambda_2 x_0) \\
&\quad + \lambda_3^3 M_3 \sin(\lambda_3 x_0) + \lambda_3^3 N_3 \cos(\lambda_3 x_0) + \lambda_4^3 M_4 \sin(\lambda_4 x_0) + \lambda_4^3 N_4 \cos(\lambda_4 x_0), \qquad (6.20)\\
w_8 &= \lambda_1^3 M_1 \cos(\lambda_1 x_0) - \lambda_1^3 N_1 \sin(\lambda_1 x_0) + \lambda_2^3 M_2 \cos(\lambda_2 x_0) - \lambda_2^3 N_2 \sin(\lambda_2 x_0) \\
&\quad + \lambda_3^3 M_3 \cos(\lambda_3 x_0) - \lambda_3^3 N_3 \sin(\lambda_3 x_0) + \lambda_4^3 M_4 \cos(\lambda_4 x_0) - \lambda_4^3 N_4 \sin(\lambda_4 x_0). \qquad (6.21)
\end{aligned}$$

Following certain algebraic manipulations, we acquire the subsequent set of equations:

$$\left.\begin{aligned}
M_1 = \frac{Q_1}{Q_9}, \quad M_2 = \frac{Q_2}{Q_{10}}, \quad M_3 = \frac{Q_3}{Q_{11}}, \quad M_4 = \frac{Q_4}{Q_{12}}, \\
N_1 = \frac{Q_5}{Q_9}, \quad N_2 = \frac{Q_6}{Q_{10}}, \quad N_3 = \frac{Q_7}{Q_{11}}, \quad N_4 = \frac{Q_8}{Q_{12}},
\end{aligned}\right\} \qquad (6.22)$$

where

$$\begin{aligned}
Q_1 = \sin(\lambda_1 x_0) &\left[\begin{array}{c} (\lambda_2 - \lambda_4)\left(w_7 - w_3\lambda_4^2 + (w_1\lambda_3\lambda_4 - w_3\lambda_3)(\lambda_3 + \lambda_4)\right) \\ -(w_5 - w_3\lambda_3 - w_3\lambda_4 + w_1\lambda_3\lambda_4)\left(\lambda_2^2 + \lambda_2\lambda_3 - \lambda_3\lambda_4 - \lambda_4^2\right) \end{array} \right] \\
+ \cos(\lambda_1 x_0) &\left[\begin{array}{c} (\lambda_2 - \lambda_4)\left(w_8 - w_4\lambda_4^2 + (w_2\lambda_3\lambda_4 - w_4\lambda_3)(\lambda_3 + \lambda_4)\right) \\ -(w_6 - w_4\lambda_3 - w_4\lambda_4 + w_2\lambda_3\lambda_4)\left(\lambda_2^2 + \lambda_2\lambda_3 - \lambda_3\lambda_4 - \lambda_4^2\right) \end{array} \right], \qquad (6.23)
\end{aligned}$$

https://doi.org/10.1017/S0022377824001673 Published online by Cambridge University Press

$$Q_2 = \sin(\lambda_2 x_0)\left[\begin{array}{c}(\lambda_1-\lambda_4)\left(w_7 - w_3\lambda_4^2 + (w_1\lambda_3\lambda_4 - w_3\lambda_3)(\lambda_3+\lambda_4)\right)\\ -(w_5 - w_3\lambda_3 - w_3\lambda_4 + w_1\lambda_3\lambda_4)\left(\lambda_1^2+\lambda_1\lambda_3-\lambda_3\lambda_4-\lambda_4^2\right)\end{array}\right] + \cos(\lambda_2 x_0)\left[\begin{array}{c}(\lambda_1-\lambda_4)\left(w_8 - w_4\lambda_4^2 + (w_2\lambda_3\lambda_4 - w_4\lambda_3)(\lambda_3+\lambda_4)\right)\\ -(w_6 - w_4\lambda_3 - w_4\lambda_4 + w_2\lambda_3\lambda_4)\left(\lambda_1^2+\lambda_1\lambda_3-\lambda_3\lambda_4-\lambda_4^2\right)\end{array}\right], \tag{6.24}$$

$$Q_3 = \sin(\lambda_3 x_0)\left[\begin{array}{c}(\lambda_4-\lambda_2)\left(w_7 - w_3\lambda_2^2 + (w_1\lambda_1\lambda_2 - w_3\lambda_1)(\lambda_2+\lambda_1)\right)\\ -(w_5 - w_3\lambda_1 - w_3\lambda_2 + w_1\lambda_1\lambda_2)\left(\lambda_4^2+\lambda_1\lambda_4-\lambda_1\lambda_2-\lambda_2^2\right)\end{array}\right] + \cos(\lambda_3 x_0)\left[\begin{array}{c}(\lambda_4-\lambda_2)\left(w_8 - w_4\lambda_2^2 + (w_2\lambda_1\lambda_2 - w_4\lambda_1)(\lambda_2+\lambda_1)\right)\\ -(w_6 - w_4\lambda_1 - w_4\lambda_2 + w_2\lambda_1\lambda_2)\left(\lambda_4^2+\lambda_1\lambda_4-\lambda_1\lambda_2-\lambda_2^2\right)\end{array}\right], \tag{6.25}$$

$$Q_4 = \sin(\lambda_4 x_0)\left[\begin{array}{c}(\lambda_3-\lambda_2)\left(w_7 - w_3\lambda_2^2 + (w_1\lambda_1\lambda_2 - w_3\lambda_1)(\lambda_2+\lambda_1)\right)\\ -(w_5 - w_3\lambda_1 - w_3\lambda_2 + w_1\lambda_1\lambda_2)\left(\lambda_3^2+\lambda_1\lambda_3-\lambda_1\lambda_2-\lambda_2^2\right)\end{array}\right] + \cos(\lambda_4 x_0)\left[\begin{array}{c}(\lambda_3-\lambda_2)\left(w_8 - w_4\lambda_2^2 + (w_2\lambda_1\lambda_2 - w_4\lambda_1)(\lambda_2+\lambda_1)\right)\\ -(w_6 - w_4\lambda_1 - w_4\lambda_2 + w_2\lambda_1\lambda_2)\left(\lambda_3^2+\lambda_1\lambda_3-\lambda_1\lambda_2-\lambda_2^2\right)\end{array}\right], \tag{6.26}$$

$$Q_5 = \cos(\lambda_1 x_0)\left[\begin{array}{c}(\lambda_2-\lambda_4)\left(w_7 - w_3\lambda_4^2 + (w_1\lambda_3\lambda_4 - w_3\lambda_3)(\lambda_3+\lambda_4)\right)\\ -(w_5 - w_3\lambda_3 - w_3\lambda_4 + w_1\lambda_3\lambda_4)\left(\lambda_2^2+\lambda_2\lambda_3-\lambda_3\lambda_4-\lambda_4^2\right)\end{array}\right] - \sin(\lambda_1 x_0)\left[\begin{array}{c}(\lambda_2-\lambda_4)\left(w_8 - w_4\lambda_4^2 + (w_2\lambda_3\lambda_4 - w_4\lambda_3)(\lambda_3+\lambda_4)\right)\\ -(w_6 - w_4\lambda_3 - w_4\lambda_4 + w_2\lambda_3\lambda_4)\left(\lambda_2^2+\lambda_2\lambda_3-\lambda_3\lambda_4-\lambda_4^2\right)\end{array}\right], \tag{6.27}$$

$$Q_6 = \cos(\lambda_2 x_0)\left[\begin{array}{c}(\lambda_1-\lambda_4)\left(w_7 - w_3\lambda_4^2 + (w_1\lambda_3\lambda_4 - w_3\lambda_3)(\lambda_3+\lambda_4)\right)\\ -(w_5 - w_3\lambda_3 - w_3\lambda_4 + w_1\lambda_3\lambda_4)\left(\lambda_1^2+\lambda_1\lambda_3-\lambda_3\lambda_4-\lambda_4^2\right)\end{array}\right] - \sin(\lambda_2 x_0)\left[\begin{array}{c}(\lambda_1-\lambda_4)\left(w_8 - w_4\lambda_4^2 + (w_2\lambda_3\lambda_4 - w_4\lambda_3)(\lambda_3+\lambda_4)\right)\\ -(w_6 - w_4\lambda_3 - w_4\lambda_4 + w_2\lambda_3\lambda_4)\left(\lambda_1^2+\lambda_1\lambda_3-\lambda_3\lambda_4-\lambda_4^2\right)\end{array}\right], \tag{6.28}$$

$$Q_7 = \cos(\lambda_3 x_0)\left[\begin{array}{c}(\lambda_4-\lambda_2)\left(w_7 - w_3\lambda_2^2 + (w_1\lambda_1\lambda_2 - w_3\lambda_1)(\lambda_2+\lambda_1)\right)\\ -(w_5 - w_3\lambda_1 - w_3\lambda_2 + w_1\lambda_1\lambda_2)\left(\lambda_4^2+\lambda_1\lambda_4-\lambda_1\lambda_2-\lambda_2^2\right)\end{array}\right] - \sin(\lambda_3 x_0)\left[\begin{array}{c}(\lambda_4-\lambda_2)\left(w_8 - w_4\lambda_2^2 + (w_2\lambda_1\lambda_2 - w_4\lambda_1)(\lambda_2+\lambda_1)\right)\\ -(w_6 - w_4\lambda_1 - w_4\lambda_2 + w_2\lambda_1\lambda_2)\left(\lambda_4^2+\lambda_1\lambda_4-\lambda_1\lambda_2-\lambda_2^2\right)\end{array}\right], \tag{6.29}$$

$$Q_8 = \cos(\lambda_4 x_0)\left[\begin{array}{c}(\lambda_3-\lambda_2)\left(w_7 - w_3\lambda_2^2 + (w_1\lambda_1\lambda_2 - w_3\lambda_1)(\lambda_2+\lambda_1)\right)\\ -(w_5 - w_3\lambda_1 - w_3\lambda_2 + w_1\lambda_1\lambda_2)\left(\lambda_3^2+\lambda_1\lambda_3-\lambda_1\lambda_2-\lambda_2^2\right)\end{array}\right] - \sin(\lambda_4 x_0)\left[\begin{array}{c}(\lambda_3-\lambda_2)\left(w_8 - w_4\lambda_2^2 + (w_2\lambda_1\lambda_2 - w_4\lambda_1)(\lambda_2+\lambda_1)\right)\\ -(w_6 - w_4\lambda_1 - w_4\lambda_2 + w_2\lambda_1\lambda_2)\left(\lambda_3^2+\lambda_1\lambda_3-\lambda_1\lambda_2-\lambda_2^2\right)\end{array}\right], \tag{6.30}$$

$$Q_9 = (\lambda_1-\lambda_3)\left(\lambda_1^2\lambda_2 - \lambda_1\lambda_2^2 + \lambda_2^2\lambda_4 - \lambda_2\lambda_4^2 + \lambda_1\lambda_4^2 - \lambda_1^2\lambda_4\right), \tag{6.31}$$

$$Q_{10} = (\lambda_2-\lambda_3)\left(\lambda_2^2\lambda_1 - \lambda_2\lambda_1^2 + \lambda_1^2\lambda_4 - \lambda_1\lambda_4^2 + \lambda_2\lambda_4^2 - \lambda_2^2\lambda_4\right), \tag{6.32}$$

$$Q_{11} = (\lambda_3-\lambda_1)\left(\lambda_2^2\lambda_3 - \lambda_2\lambda_3^2 - \lambda_2^2\lambda_4 + \lambda_2\lambda_4^2 - \lambda_3\lambda_4^2 + \lambda_3^2\lambda_4\right), \tag{6.33}$$

$$Q_{12} = (\lambda_4-\lambda_1)\left(\lambda_3^2\lambda_2 - \lambda_3\lambda_2^2 + \lambda_2^2\lambda_4 - \lambda_2\lambda_4^2 + \lambda_3\lambda_4^2 - \lambda_3^2\lambda_4\right). \tag{6.34}$$

https://doi.org/10.1017/S0022377824001673 Published online by Cambridge University Press

In this arrangement, a greater number of boundary conditions is used compared with the uncomplicated slab geometry. These additional conditions introduce an additional degree of freedom, providing a more effective means of system control. The entire system can be managed with increased efficiency. Modifying the magnetic field, which is contingent on the Beltrami parameter and density ratio, within the inner slab allows for straightforward control over the structure's characteristics. Adjusting the length of the inner slab can reduce the pressure inside. In contrast, in the case of the simple slab geometry, the application of additional boundary conditions is not feasible, resulting in challenges in controlling the nature of the relaxed structure at the system's centre.

7. Numerical results

The inherent magnetic field is a fundamental characteristic of a planet. Beyond influencing the electromagnetic conditions surrounding a planetary body, it acts as a crucial indicator of the internal structure and dynamics of the host planet (Cao *et al.* 2020). The presence of a robust planetary-scale magnetic field is likely the result of dynamo action occurring within the planet. This process requires a large amount of electrically conductive fluid and involves rapid and intricate-moving fluid motions within the planet's interior. These movements help generate and maintain the magnetic field. In this current study, our focus is on investigating the dynamo action within Saturn. To achieve this, our numerical investigation relies on observational data from Saturn's E-ring (Wahlund *et al.* 2009; Shohaib *et al.* 2022), with the plasma parameters having the following specified values: $m_d = 4 \times 10^{-15}$ kg, $n_{s_e} = (2 - -7) \times 10^7$ m^{-3}, $n_{s_d} = 10^4 - -10^5$ m^{-3} and $Z_d = 10^2$. In the present work, the velocities were normalized by a characteristic velocity, such as the Alfvén velocity V_A, and the distances were normalized by the electron skin depth λ_{s_e}. Thus, the plotted values are dimensionless.

7.1. *Plasma flow and dynamo action*

Dynamo processes are now widely accepted as the primary origin of magnetic fields in many astrophysical settings. This section will explore the features of the magnetic field and flow field of the relaxed structures within Saturn's E-ring a three-component dusty plasma (Wahlund *et al.* 2009; Shohaib *et al.* 2022), considering both configurations – simple rectangular geometry and coplanar rectangular geometry. The analysis will primarily focus on examining the impact of Beltrami parameters on the characteristics of self-organized structures. The graphs are generated with a fixed value of $x = 5$, representing the length of the rectangle, in the case of simple rectangular geometry. Meanwhile, for coplanar rectangular geometry, the graphs are plotted with $x_0 = 2$, representing the length of the inner rectangular slab along the x-axis, and $x = 5$, representing the length of the outer rectangular slab along the x-axis. Figures 1–2 exhibit the fluctuations in the magnetic and velocity profiles concerning the Beltrami parameter $a_{s_e} = 25.7$, $a_{s_i} = 0.1$ and $a_{s_d} = 1.0$ and figures 3–4 are plotted for a different set of Beltrami parameters $a_{s_e} = 0.7$, $a_{s_i} = 1.4$ and $a_{s_d} = 50.9$. Figures 1 and 3 depicting the magnetic field and velocity profiles are presented for the solution of the quadruple Beltrami state within a straightforward rectangular configuration and figures 2–4 illustrating the magnetic field and velocity profiles are generated to showcase the solution of the quadruple Beltrami state in a rectangular configuration featuring an internal rectangular slab.

The magnetic field and flow field behave differently in these two cases, indicating distinct dynamo mechanisms.

https://doi.org/10.1017/S0022377824001673 Published online by Cambridge University Press

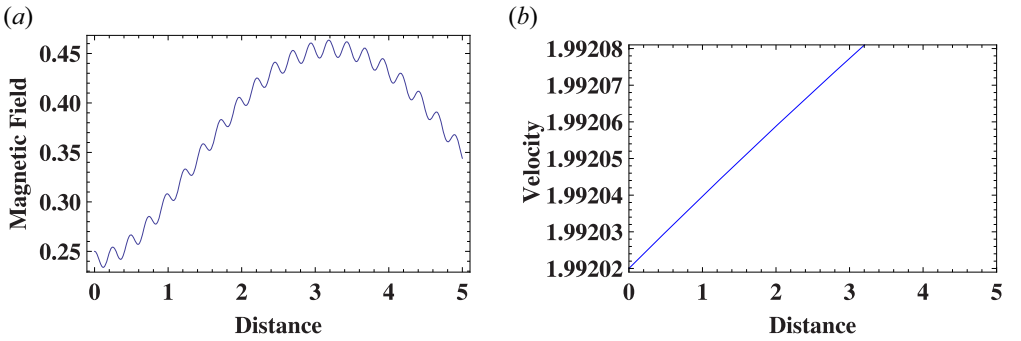

FIGURE 1. Magnetic field and velocity profiles are plotted for the solution of quadruple Beltrami state in a simple rectangular configuration. The Beltrami parameters are $a_{s_e} = 25.7$, $a_{s_i} = 0.1$ and $a_{s_d} = 1.0$. The associated scale parameters are $\lambda_1 = 25.661$, $\lambda_2 = 0.050553$, $\lambda_3 = 1.0$ and $\lambda_4 = 0.0884166$.

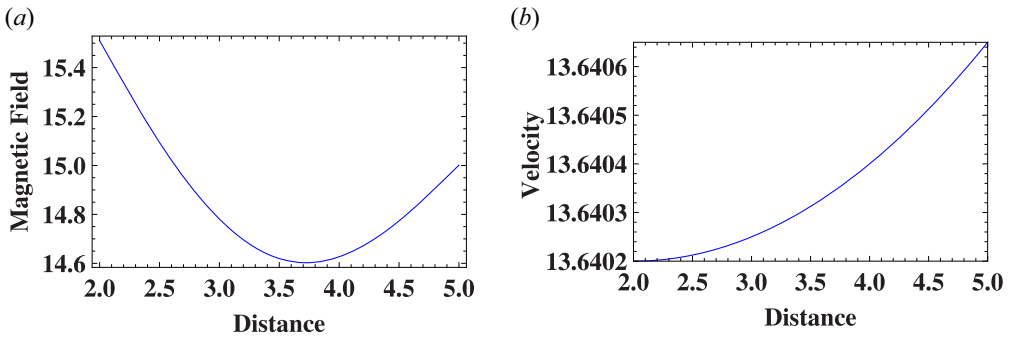

FIGURE 2. Magnetic field and Velocity profiles are plotted for the solution of quadruple Beltrami state in a rectangular configuration with an internal conductor. The Beltrami parameters are $a_{s_e} = 25.7$, $a_{s_i} = 0.1$ and $a_{s_d} = 1.0$. The associated scale parameters are $\lambda_1 = 25.661$, $\lambda_2 = 0.050553$, $\lambda_3 = 1.0$ and $\lambda_4 = 0.0884166$.

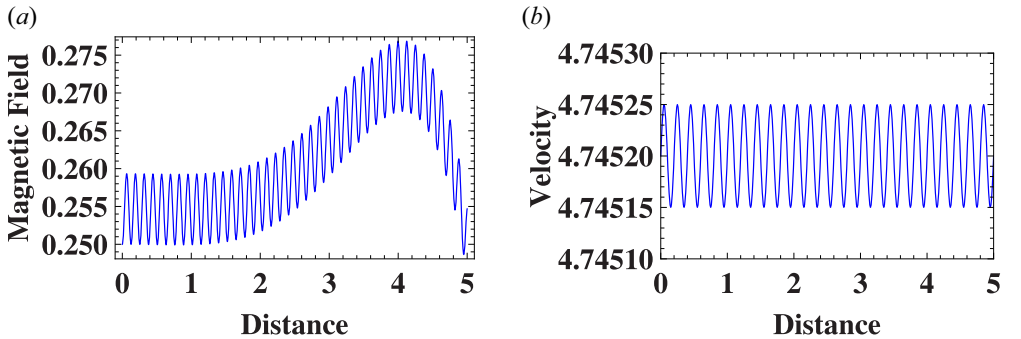

FIGURE 3. Magnetic field and velocity profiles are plotted for the solution of quadruple Beltrami state in a simple rectangular configuration. The Beltrami parameters are $a_{s_e} = 0.7$, $a_{s_i} = 1.4$ and $a_{s_d} = 50.9$. The associated scale parameters are $\lambda_1 = 50.9$, $\lambda_2 = 1.3998$, $\lambda_3 = 0.350101 + 0.936942i$ and $\lambda_4 = 0.350101 - 0.936942i$.

https://doi.org/10.1017/S0022377824001673 Published online by Cambridge University Press

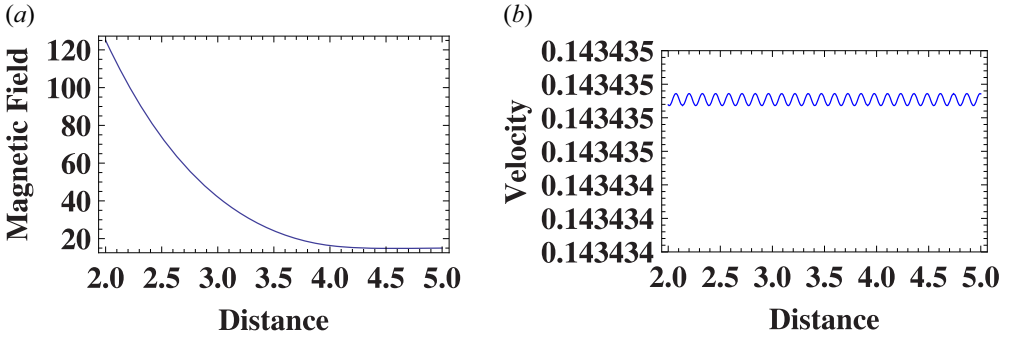

FIGURE 4. Magnetic field and velocity profiles are plotted for the solution of quadruple Beltrami state in a rectangular configuration with an internal conductor. The Beltrami parameters are $a_{s_e} = 0.7$, $a_{s_i} = 1.4$ and $a_{s_d} = 50.9$. The associated scale parameters are $\lambda_1 = 50.9$, $\lambda_2 = 1.3998$, $\lambda_3 = 0.350101 + 0.936942i$ and $\lambda_4 = 0.350101 - 0.936942i$.

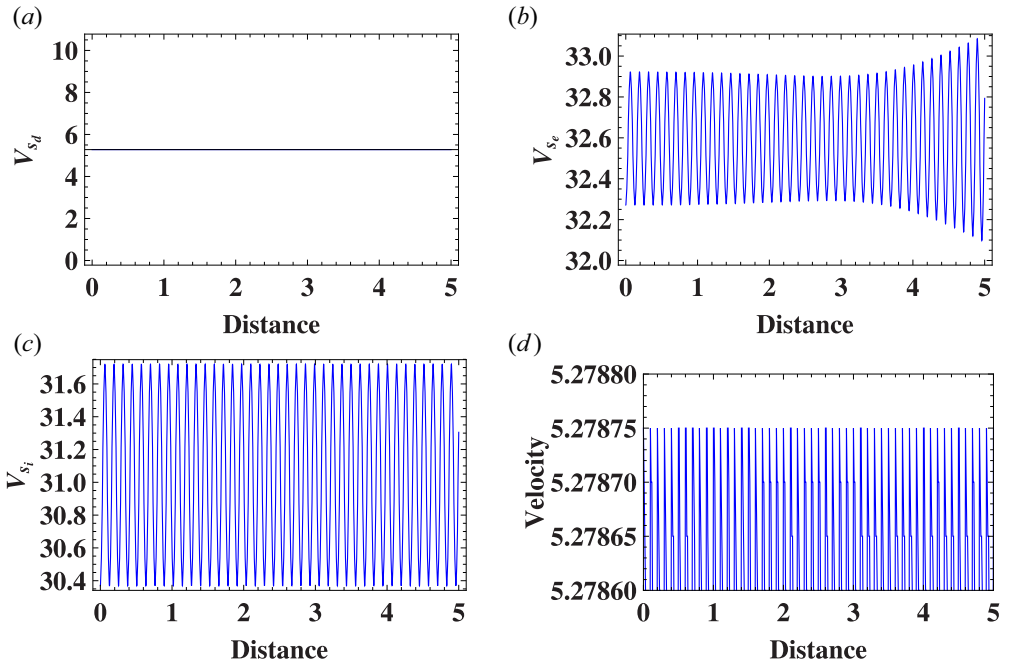

FIGURE 5. Velocities (velocity of dust particle V_{s_d}, electrons V_{s_e}, ions V_{s_i} and composite velocity V) profiles are plotted for the solution of quadruple Beltrami state in a simple rectangular configuration. The Beltrami parameters are $a_{s_e} = 0.7$, $a_{s_i} = 1.5$ and $a_{s_d} = 50.9$. The associated scale parameters are $\lambda_1 = 50.9$, $\lambda_2 = 1.49979$, $\lambda_3 = 0.350104 + 0.9369271i$ and $\lambda_4 = 0.350104 - 0.9369271i$.

7.1.1. *Saturn's magnetosphere*

Magnetic field < flow field: in this scenario, shown in figures 1 and 3, the magnetic field is weaker than the flow field. This suggests the presence of a fast dynamo. In such environments, where the flow dominates the magnetic field, turbulent or rapid fluid motions can stretch, fold and amplify the magnetic field efficiently, which is characteristic of a fast dynamo (Vainshtein & Rosner 1991). Although altering the Beltrami

https://doi.org/10.1017/S0022377824001673 Published online by Cambridge University Press

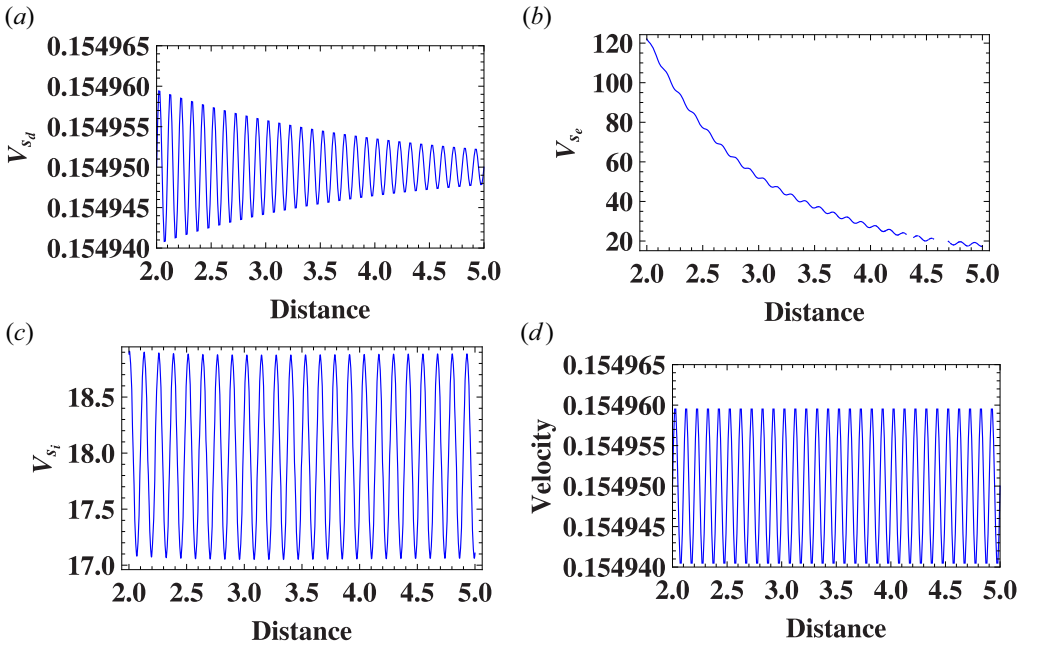

FIGURE 6. Velocities (velocity of dust particle V_{s_d}, electrons V_{s_e}, ions V_{s_i} and composite velocity V) profiles are plotted for the solution of quadruple Beltrami state in a rectangular configuration with an internal conductor. The Beltrami parameters are $a_{s_e} = 0.7$, $a_{s_i} = 1.5$ and $a_{s_d} = 50.9$. The associated scale parameters are $\lambda_1 = 50.9$, $\lambda_2 = 1.49979$, $\lambda_3 = 0.350104 + 0.9369271i$ and $\lambda_4 = 0.350104 - 0.9369271i$.

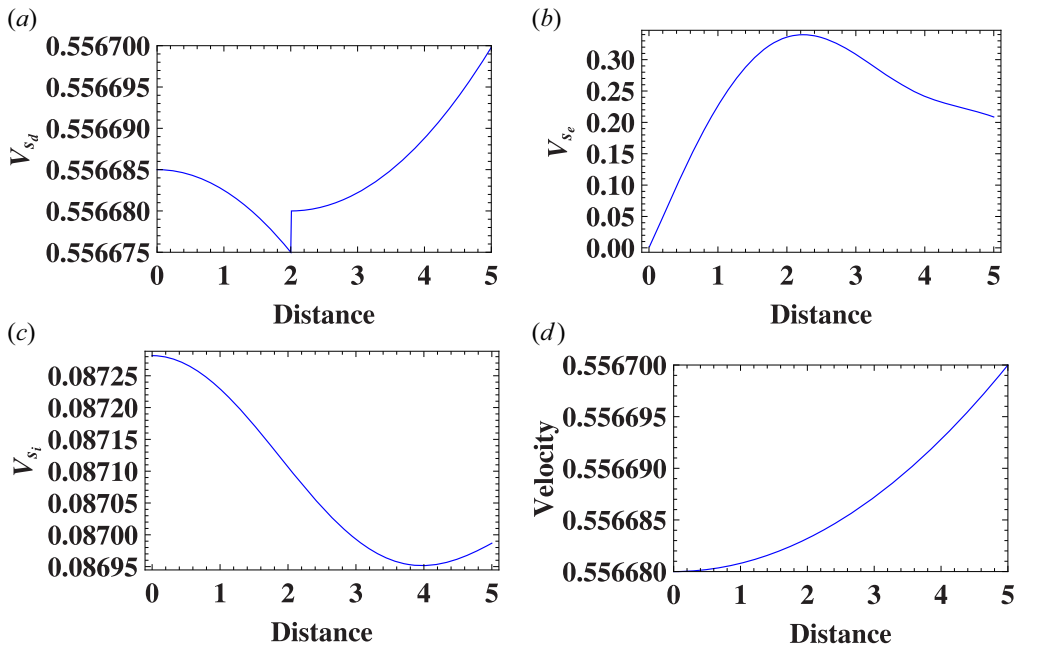

FIGURE 7. Velocities (velocity of dust particle V_{s_d}, electrons V_{s_e}, ions V_{s_i} and composite velocity V) profiles are plotted for the solution of quadruple Beltrami state in a simple rectangular configuration. The Beltrami parameters are $a_{s_e} = 2.7$, $a_{s_i} = 1.3$ and $a_{s_d} = 0.9$. The associated scale parameters are $\lambda_1 = 2.25706$, $\lambda_2 = 0.443913$, $\lambda_3 = 1.29902$ and $\lambda_4 = 0.9$.

https://doi.org/10.1017/S0022377824001673 Published online by Cambridge University Press

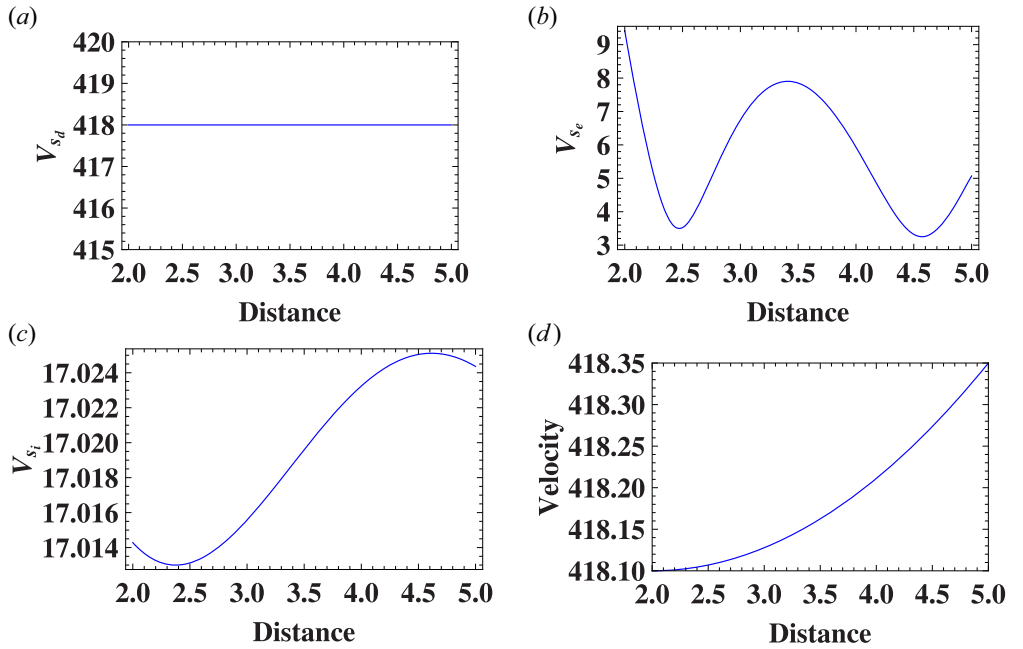

FIGURE 8. Velocities (velocity of dust particle V_{s_d}, electrons V_{s_e}, ions V_{s_i} and composite velocity V) profiles are plotted for the solution of the quadruple Beltrami state in a rectangular configuration with an internal conductor. The Beltrami parameters are $a_{s_e} = 2.7$, $a_{s_i} = 1.3$ and $a_{s_d} = 0.9$. The associated scale parameters are $\lambda_1 = 2.25706$, $\lambda_2 = 0.443913$, $\lambda_3 = 1.29902$ and $\lambda_4 = 0.9$.

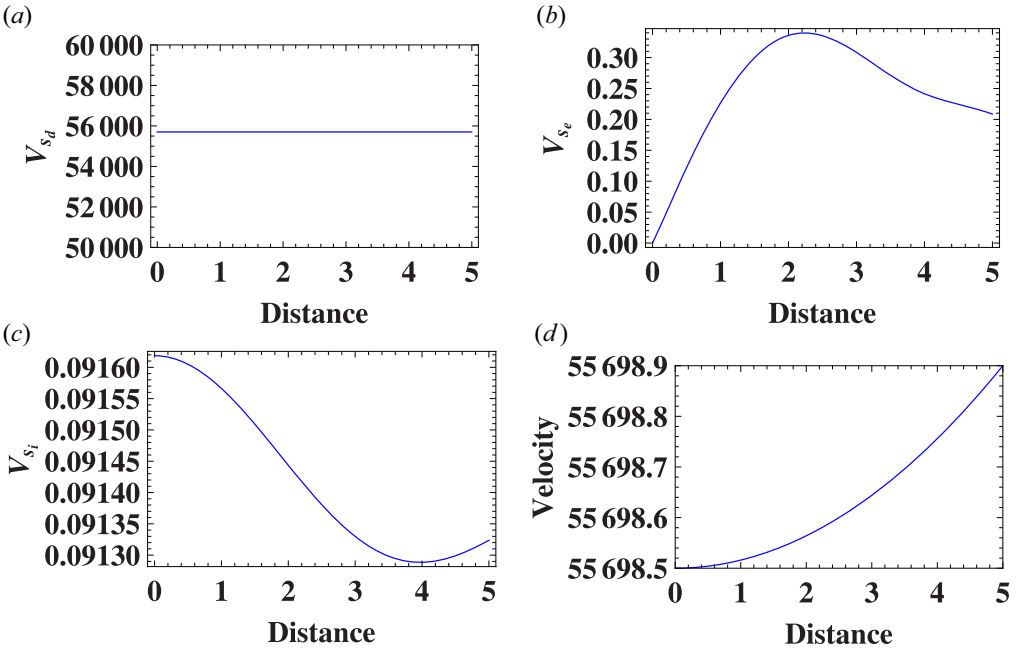

FIGURE 9. Velocities (velocity of dust particle V_{s_d}, electrons V_{s_e}, ions V_{s_i} and composite velocity V) profiles are plotted for the solution of quadruple Beltrami state in a simple rectangular configuration. The densities of plasma species are $n_{s_e} = 2 \times 10^9$, $n_{s_i} = 2 \times 10^9$, $n_{s_d} = 10^1$ and $z_d = 10^2$.

https://doi.org/10.1017/S0022377824001673 Published online by Cambridge University Press

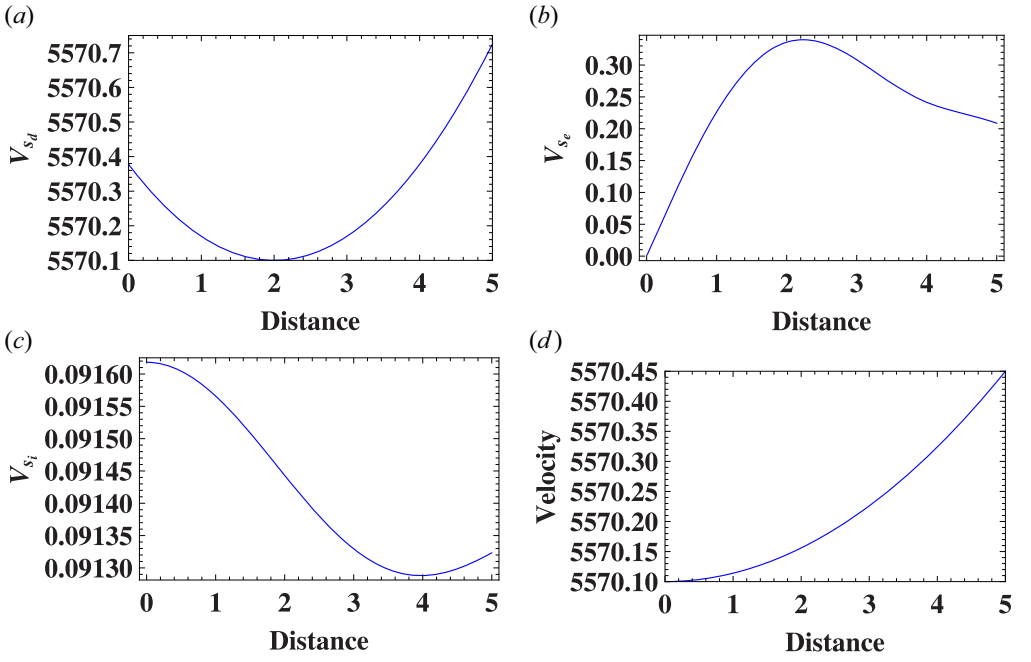

FIGURE 10. Velocities (velocity of dust particle V_{s_d}, electrons V_{s_e}, ions V_{s_i} and composite velocity V) profiles are plotted for the solution of the quadruple Beltrami state in a simple rectangular configuration. The density of plasma species are $n_{s_e} = 2 \times 10^9$, $n_{s_i} = 2 \times 10^9$, $n_{s_d} = 10^2$ and $z_d = 10^2$.

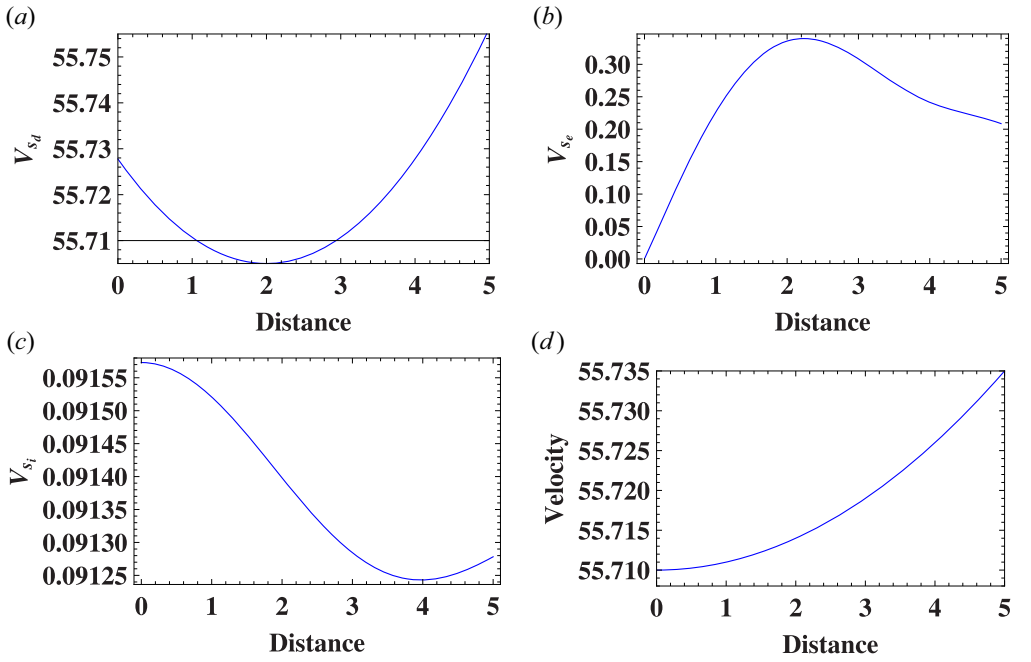

FIGURE 11. Velocities (velocity of dust particle V_{s_d}, electrons V_{s_e}, ions V_{s_i} and composite velocity V) profiles are plotted for the solution of the quadruple Beltrami state in a simple rectangular configuration. The density of plasma species are $n_{s_e} = 2 \times 10^8$, $n_{s_i} = 2 \times 10^8$, $n_{s_d} = 10^3$ and $z_d = 10^2$.

https://doi.org/10.1017/S0022377824001673 Published online by Cambridge University Press

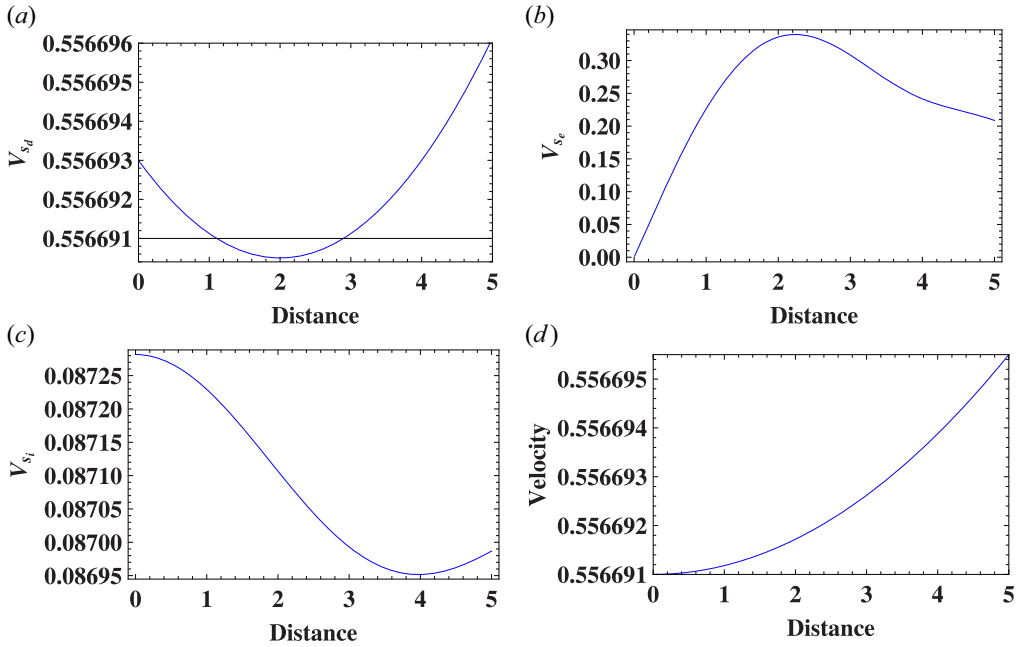

FIGURE 12. Velocities (velocity of dust particle V_{s_d}, electrons V_{s_e}, ions V_{s_i} and composite velocity V) profiles are plotted for the solution of the quadruple Beltrami state in a simple rectangular configuration. The density of plasma species are $n_{s_e} = 2 \times 10^7$, $n_{s_i} = 2 \times 10^7$, $n_{s_d} = 10^4$ and $z_d = 10^2$.

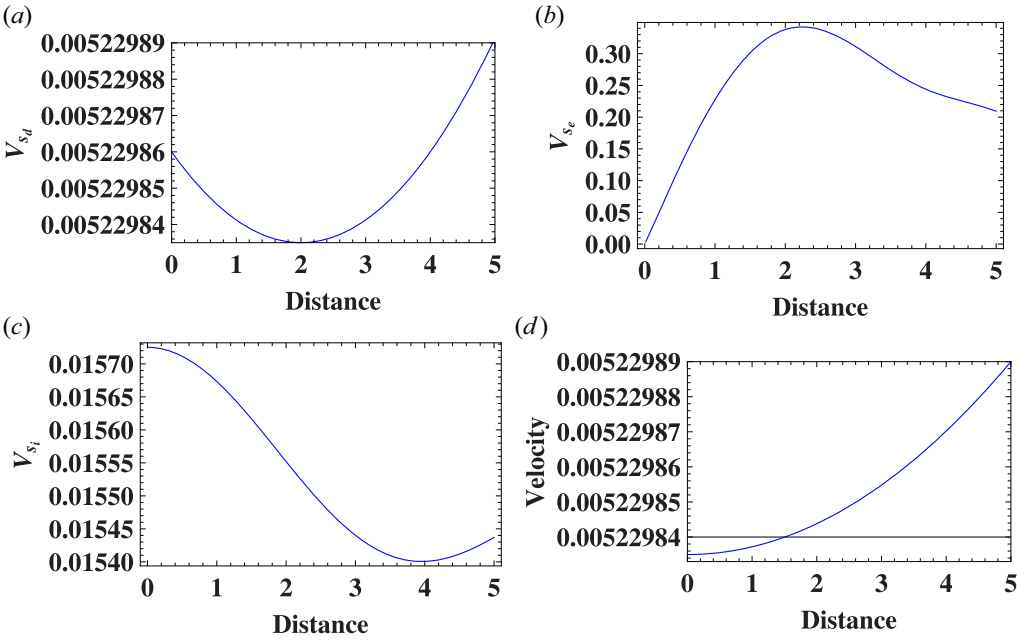

FIGURE 13. Velocities (velocity of dust particle V_{s_d}, electrons V_{s_e}, ions V_{s_i} and composite velocity V) profiles are plotted for the solution of the quadruple Beltrami state in a simple rectangular configuration. The density of plasma species are $n_{s_e} = 2 \times 10^6$, $n_{s_i} = 2 \times 10^7$, $n_{s_d} = 10^5$ and $z_d = 10^2$.

https://doi.org/10.1017/S0022377824001673 Published online by Cambridge University Press

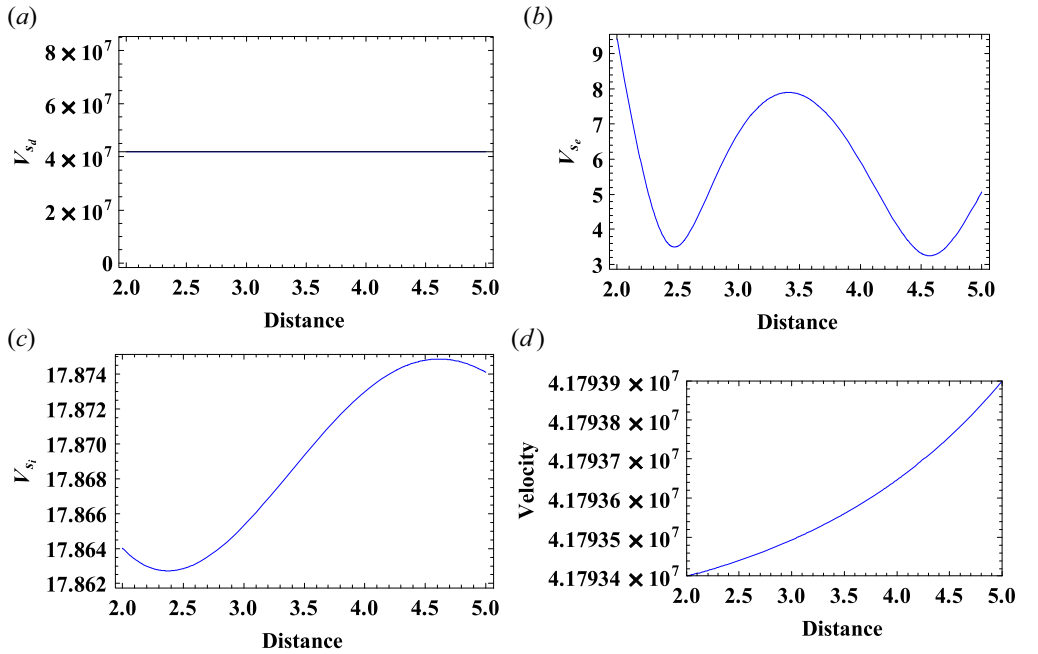

FIGURE 14. Velocities (velocity of dust particle V_{s_d}, electrons V_{s_e}, ions V_{s_i} and composite velocity V) profiles are plotted for the solution of the quadruple Beltrami state in a rectangular configuration with an internal conductor. The density of plasma species are $n_{s_e} = 2 \times 10^9$, $n_{s_i} = 2 \times 10^9$, $n_{s_d} = 10^1$ and $z_d = 10^2$.

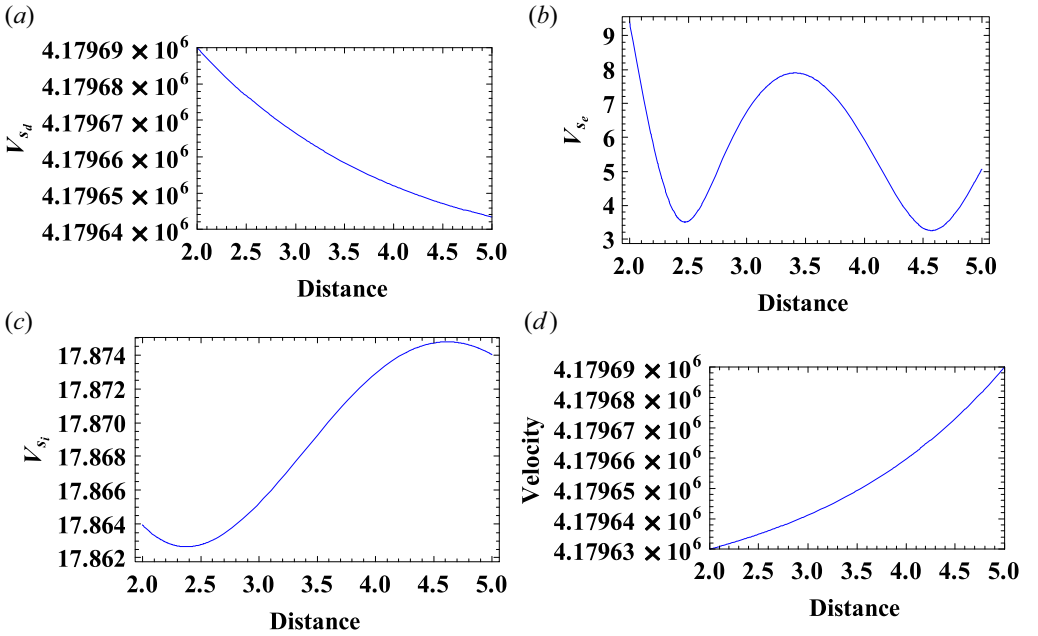

FIGURE 15. Velocities (velocity of dust particle V_{s_d}, electrons V_{s_e}, ions V_{s_i} and composite velocity V) profiles are plotted for the solution of the quadruple Beltrami state in a rectangular configuration with an internal conductor. The density of plasma species are $n_{s_e} = 2 \times 10^9$, $n_{s_i} = 2 \times 10^9$, $n_{s_d} = 10^2$ and $z_d = 10^2$.

https://doi.org/10.1017/S0022377824001673 Published online by Cambridge University Press

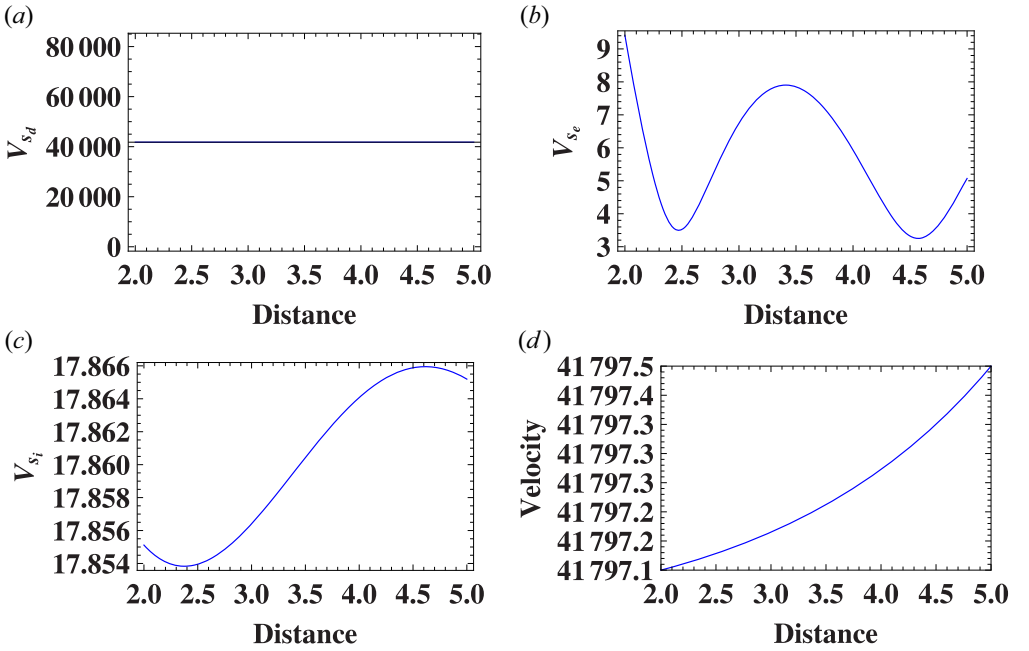

FIGURE 16. Velocities (velocity of dust particle V_{s_d}, electrons V_{s_e}, ions V_{s_i} and composite velocity V) profiles are plotted for the solution of the quadruple Beltrami state in a rectangular configuration with an internal conductor. The density of plasma species are $n_{s_e} = 2 \times 10^8$, $n_{s_i} = 2 \times 10^8$, $n_{s_d} = 10^3$ and $z_d = 10^2$.

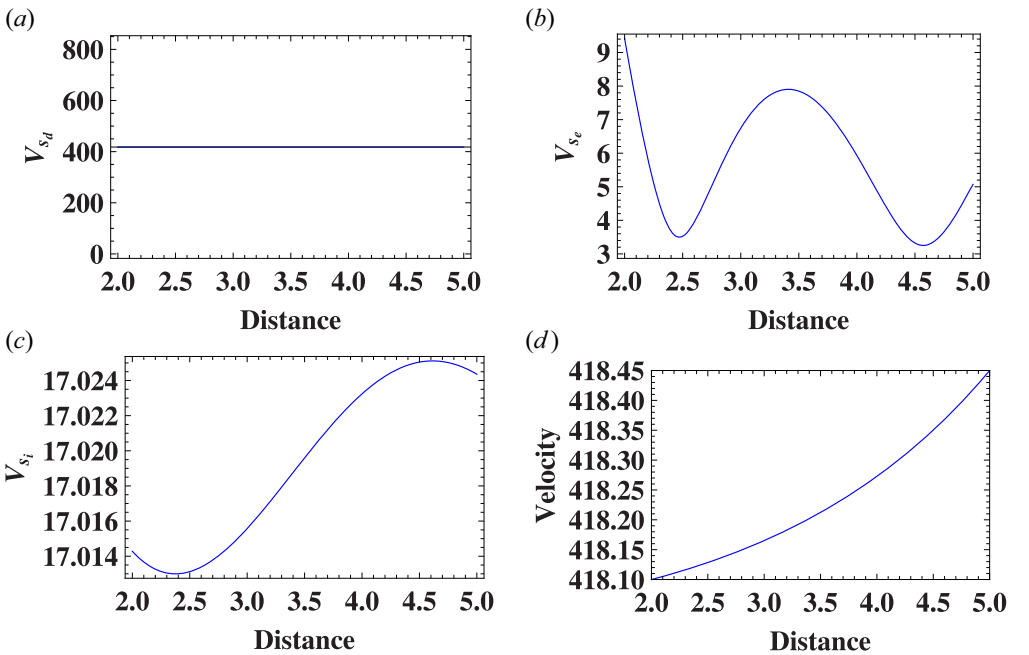

FIGURE 17. Velocities (velocity of dust particle V_{s_d}, electrons V_{s_e}, ions V_{s_i} and composite velocity V) profiles are plotted for the solution of the quadruple Beltrami state in a rectangular configuration with an internal conductor. The density of plasma species are $n_{s_e} = 2 \times 10^7$, $n_{s_i} = 2 \times 10^7$, $n_{s_d} = 10^4$ and $z_d = 10^2$.

https://doi.org/10.1017/S0022377824001673 Published online by Cambridge University Press

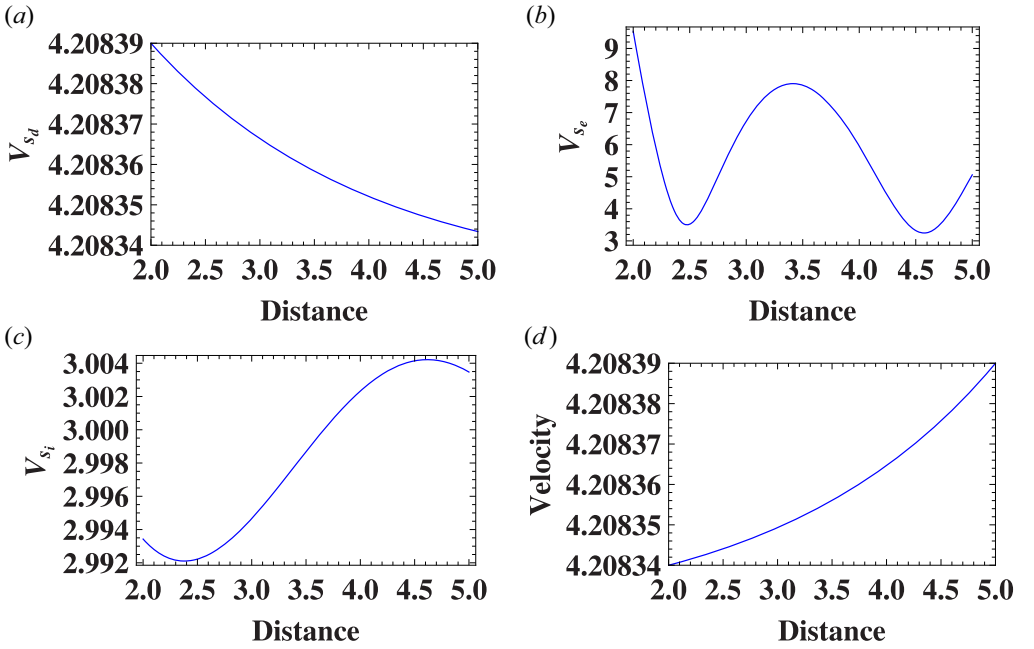

FIGURE 18. Velocities (velocity of dust particle V_{s_d}, electrons V_{s_e}, ions V_{s_i} and composite velocity V) profiles are plotted for the solution of the quadruple Beltrami state in a rectangular configuration with an internal conductor. The density of plasma species are $n_{s_e} = 2 \times 10^6$, $n_{s_i} = 2 \times 10^7$, $n_{s_d} = 10^5$ and $z_d = 10^2$.

parameters from $a_{s_e} = 25.7$, $a_{s_i} = 0.1$ and $a_{s_d} = 1.0$ to $a_{s_e} = 0.7$, $a_{s_i} = 1.4$ and $a_{s_d} = 50.9$ results in a transformation of the corresponding scale parameters from real $\lambda_1 = 25.661$, $\lambda_2 = 0.050553$, $\lambda_3 = 1.0$ and $\lambda_4 = 0.0884166$ to complex conjugate $\lambda_1 = 50.9$, $\lambda_2 = 1.3998$, $\lambda_3 = 0.350101 + 0.936942i$ and $\lambda_4 = 0.350101 - 0.936942i$, while the inherent characteristics of the magnetic and flow fields remain unchanged.

7.1.2. *Saturn's E ring*

Magnetic field > flow field: in this case, illustrated in figures 2 and 4, the magnetic field is stronger than the flow field, which may favour a slow dynamo (Soward 1990). A stronger magnetic field leads to more organized and less turbulent interactions with the flow, resulting in slower amplification of the magnetic field. Figures 2 and 4 are plotted using the same Beltrami parameters as figures 1 and 3, respectively. Moreover, the magnetic field in figure 4 demonstrates a scale significantly exceeding that of the driving flow, it identifies a large-scale dynamo (Brandenburg 2009). The field strength is significantly higher here, not only due to the influence of the flow field, but also because of the internal conductor, resulting in a much stronger magnetic field than in the simple rectangular geometry. It indicates that altering the Beltrami parameters in the scenario of a rectangular configuration with an internal conductor can result in the dynamo transitioning between fast dynamo and slow dynamo, or *vice versa*.

7.2. *Velocities profiles of the plasma species*

Within this section, we showcase the velocity profiles of distinct plasma constituents – namely, electrons, ions and negatively charged dust particles – along with the unified velocity. The velocity profiles for electrons V_{s_e}, ions V_{s_i} and negatively charged dust particles V_{s_d} are graphed in accordance with (3.5), (2.11) and (3.6), respectively.

https://doi.org/10.1017/S0022377824001673 Published online by Cambridge University Press

Meanwhile, the unified flow is illustrated through the useof (4.4). The analysis of the graphs is conducted for both solutions, involving a simple rectangular geometry and a rectangular configuration with an internal conductor. This examination involves the manipulation of Beltrami parameters and the densities of plasma species.

7.2.1. *Influence of Beltrami parameters*

Figures 5–6 are generated using identical Beltrami parameters $a_{s_e} = 0.7$, $a_{s_i} = 1.5$ and $a_{s_d} = 50.9$. In figure 5, velocity profiles of plasma species are illustrated within a simple rectangular geometry, while figure 6 depicts the velocities of plasma components within a rectangular configuration featuring an internal conductor. The corresponding four scale parameters are denoted as $\lambda_1 = 50.9$, $\lambda_2 = 1.49979$, $\lambda_3 = 0.350104 + 0.9369271i$ and $\lambda_4 = 0.350104 - 0.9369271i$, comprising two real values and a pair of complex conjugates. Same Beltrami parameters $a_{s_e} = 2.7$, $a_{s_i} = 1.3$ and $a_{s_d} = 0.9$ are employed in the creation of both figures 7 and 8. In figure 7, we showcase the velocity profiles of plasma species in a simple rectangular geometry, while figure 8 reveals the velocities of plasma components within a rectangular set-up featuring an internal conductor. The corresponding four scale parameters are articulated as $\lambda_1 = 2.25706$, $\lambda_2 = 0.443913$, $\lambda_3 = 1.29902$ and $\lambda_4 = 0.9$, all of which possess real values. In the scenario of a rectangular geometry with an internal conductor, it has been noted that when all the scale parameters, which are dependent on Beltrami parameters, are real, the unified flow reaches its peak magnitude (figure 8). Conversely, when the scale parameters form a pair of complex conjugates, the unified flow exhibits its minimum intensity (figure 6). This trend is reversed in the case of a simple rectangular geometry. This indicates that the Beltrami parameters exert a significant influence on the velocity of the plasma system and its constituent components.

7.2.2. *Influence of plasma species densities*

In the atmosphere of Saturn, the densities of plasma species like electrons, ions and dust particles exhibit non-uniformity, fluctuating with changes in the magnetosphere's radius. Consequently, the velocities of plasma particles are significantly impacted by the density ratios among these species. Figures 9–18 depict variations in both the unified velocity and individual velocities of plasma particles, highlighting the influence of changing plasma particle densities and keeping constant all other parameters. Figures 9–13 are generated based on the quadruple Beltrami state solution within a basic rectangular geometry, while figures 14–18 are plotted from the solution of the quadruple Beltrami state in a rectangular configuration featuring an internal conductor. The examination of these graphs reveals that the magnitudes of velocities for smaller species such as electrons and ions remain constant when altering the densities of plasma species in both configurations – whether in a simple rectangular geometry or in a rectangular geometry with an internal conductor. Conversely, the velocity magnitude of dust particles is markedly influenced by the density ratio of plasma particles. It reaches its maximum, as shown in figures 9 and 14, when electron density is at its highest, $n_{s_e} = 2 \times 10^9$, and the density of negatively charged dust particles is at its lowest, $n_{s_d} = 10$. Conversely, its magnitude diminishes shown in figures 13 and 18 when electron density decreases, $n_{s_e} = 2 \times 10^6$,and the density of dust particles increases, $n_{s_d} = 10^5$. Since the unified velocity is a composite of the velocities velocities of electrons, ions and dust particles, the unified velocity attains its maximum value when the velocity strength of dust particles is at its peak, and conversely, it decreases when the velocity of dust particles diminishes. Furthermore, the total magnitude of the unified velocity is higher in the scenario of a rectangular geometry with an internal conductor compared with the velocity strength in a simple rectangular configuration. This observation indicates that the

https://doi.org/10.1017/S0022377824001673 Published online by Cambridge University Press

presence of an internal conductor has the potential to augment the velocity's intensity. This insight holds significance in elucidating the velocity dynamics of the plasma system within the Saturn magnetosphere and its rings. The trend of the magnetic profiles are strongly influenced by changing the Beltrami parameters or by varying the density of the dust particles in a simple rectangular geometry. In the above discussion for a simple rectangular configuration, it has been also observed that the associated scale parameters are real for the paramagnetic trend, but for complex scale parameters, the magnetic field becomes maximum moving away from the centre, which manifests the diamagnetic trend. This shows a clear distinction of the both geometries.

8. Concluding remarks

The relaxation phenomenon in a magnetized three-fluid dusty plasma, consisting of negatively charged dust particles, electrons and ions, has been observed. The Beltrami conditions are attained by solving the momentum-balanced equations for the three components alongside Ampere's law. A quadruple Beltrami state is derived by considering three Beltrami parameters. The helicities of dust particles, electrons and ions, along with the total energy, serve as the four constraints in the current plasma system. The quadruple curl relaxed Beltrami state is a composite of four distinct single relaxed Beltrami states, resulting in the system having four unique eigenvalues. The solutions for the relaxed state have been obtained in two distinct configurations. One corresponds to a simple rectangular geometry, and the other involves a rectangular geometry featuring an inner rectangular slab acting as an internal conductor. We have established relationships describing the unified flow and derived the individual flows of plasma particles, including electrons, ions and negatively charged dust particles. Dynamo action has been identified in the Saturn plasma, using real plasma parameters from Saturn itself. Dynamo action is discerned by varying the Beltrami parameters, exhibiting small-scale dynamo behaviour in a simple rectangular geometry and generating large-scale dynamo effects in a rectangular configuration with an internal conductor. Additionally, it has been observed that the overall strength of the magnetic field reaches its maximum in the presence of an internal conductor in the rectangular geometry.

Velocity profiles have been graphed by systematically altering the Beltrami parameters and the density of plasma species. It has been noted that the densities of smaller species, namely electrons and ions, and the density of heavier particles, negatively charged dust particles, significantly impact the description of the plasma system's flow. The unified velocity increases with a higher electron concentration and lower dust particle abundance, and *vice versa*. Similarly, the flow of dust particles is influenced by changes in density ratio in a manner consistent with the unified flow, while the overall flow of smaller species – electrons and ions – remains unaltered. These findings are valuable for elucidating the characteristics of relaxed structures and dynamo action in the context of Saturn's rings, planetary rings, rotating stars, pulsar magneto sphere and excitations in interstellar medium.

Acknowledgements

Editor Dmitri Uzdensky thanks the referees for their advice in evaluating this article.

Declaration of interests

The author reports no conflict of interest.

REFERENCES

ARNOLD, V.I. & KHESIN, B.A. 1998 *Topological Methods in Hydrodynamics*. Springer.

AVINASH, K. 1991 On toroidal equilibrium of non-neutral plasma. *Phys. Fluids* B*: Plasma Phys*. **3**, 3226–3231.

AVINASH, K. 1992 Some stationary solutions of two-fluid magnetohydrodynamic equations. *Phys. Fluids* B **4**, 3856–3862.

BHATTACHARJEE, C. & FENG, J.C. 2020*a* On Beltrami states near black hole event horizon. *Phys. Plasmas* **27**, 072901.

BHATTACHARJEE, C. & STARK, D.J. 2020*b* Vortex generation in the early Universe. *Astron. Astrophys*. **642**, L6.

BHATTACHARYYA, R., JANAKI, M.S. & DASGUPTA, B. 2003 Relaxation in electron-positron plasma: a possibility. *Phys. Lett.* A **315**, 120–125.

BRANDENBURG, A. 2009 Large-scale dynamos at low magnetic Prandtl numbers. *Astrophys. J*. **697**, 1206–1213.

CAO, H., DOUGHERTY, M.K., HUNT, G.J., PROVAN, G., COWLEY, S.W.H., BUNCE, E.J., KELLOCK, S. & STEVENSON, D.J. 2020 Evidence in Cassini magnetic field data for a deeply rotating dynamo in Saturn. *Icarus* **334**, 113541.

GOLD, T. & HOYLE, F. 1958 On the origin of solar flares. *Mon. Not. R. Acad. Sci*. **120**, 89.

GONDAL, S.M. 2020*b* Beltrami states in Earth's dusty mesosphere. *Phys. Plasmas* **27**, 113703.

GONDAL, S.M. 2022 Relaxation of multi-ion plasmas in an internal conductor. *AIP Adv*. **12**, 025202.

GONDAL, S.M. & IQBAL, M. 2020*a* Quadruple Beltrami state in electron-depleted multi-ion dusty plasmas. *Phys. Plasmas* **27**, 083702.

GONDAL, S.M. & IQBAL, M. 2020*c* The possibility of relaxation in Quadruple Beltrami states in a four-component magneto dusty plasma. *Phys. Scr*. **96**, 015602.

GONDAL, S.M. & IQBAL, M. 2021*a* Multiscale self-organized triple Beltrami states in four-component dusty plasmas. *Planet. Space Sci*. **198**, 105174.

GONDAL, S.M. & IQBAL, M. 2021*b* Formation of self-organized structures in internal conductor plasma. *Phys. Scr*. **96**, 075602.

GONDAL, S.M., IQBAL, M., KHOSA, A.H. & MURTAZA, G. 2017 Quadruple Beltrami fields in three component plasmas. *Phys. Plasmas* **24**, 062903.

GONDAL, S.M., IQBAL, M., SHAFAULLAH, ASGHAR, M. & KHOSA, A.H. 2019 Double Beltrami states and loss of equilibrium in electron, positron and ion plasmas. *J. Plasma Phys*. **85**, 905850306.

GUZDAR, P.N., MAHAJAN, S.M. & YOSHIDA, Z. 2005 A theory for the pressure pedestal in high (H) mode tokamak discharges. *Phys. Plasmas* **12**, 032502.

IQBAL, M. & SHUKLA, P.K. 2012 Relaxed magnetic field structures in multi-ion plasmas. *Astrophys. Space Sci*. **339**, 19–23.

KAGAN, D. & MAHAJAN, S.M. 2010 Application of double Beltrami states to solar eruptions. *Mon. Not. R. Astron. Soc*. **406**, 1140–1145.

MAHAJAN, S.M. 2008 Classical perfect diamagnetism: expulsion of current from the plasma interior. *Phys. Rev. Lett*. **100**, 075001.

MAHAJAN, S.M. & LINGAM, M. 2015 Multi-fluid systems—multi-Beltrami relaxed states and their implications. *Phys. Plasmas* **22**, 092123.

MAHAJAN, S.M. & LINGAM, M. 2020 Constraining Alfvénic turbulence with helicity invariants. *Mon. Not. R. Astron. Soc*. **495** (3), 2771–2776.

MAHAJAN, S.M. & YOSHIDA, Z. 1998 Double curl Beltrami flow: diamagnetic structures. *Phys. Rev. Lett*. **81**, 4863.

MAHAJAN, S.M. & YOSHIDA, Z. 2000 A collisionless self-organizing model for the high-confinement (H-mode) boundary layer. *Phys. Plasmas* **7**, 635–640.

MAHMOOD, S. & UR-REHMAN, H. 2013 Compressive and rarefactive solitons for fast and slow ion acoustic waves in multi-ion plasmas. *J. Phys. Soc. Japan*. **82**, 074501.

MIYAMOTO, K. 1980 *Plasma Physics For Nuclear Fusion*. MIT.

https://doi.org/10.1017/S0022377824001673 Published online by Cambridge University Press

NAKASHIMA, C., YOSHIDA, Z., HIMURA, H., FUKAO, M., MORIKAWA, J. & SAITOH, H. 2002 Injection of electron beam into a toroidal trap using chaotic orbits near magnetic null. *Phys. Rev.* E **65**, 036409.

NEBBAT, E. & ANNOU, R. 2010 On vortex dust structures in magnetized dusty plasmas. *Phys. Plasmas* **17**, 093702.

OGAWA, Y. 2002 On two-dimensional modeling of magnetotelluric field data. *Surv. Geophysics*. **23**, 251–273.

OHSAKI, S., SHATASHVILI, N.L., YOSHIDA, Z. & MAHAJAN, S.M. 2001 Magnetofluid coupling: eruptive events in the solar corona. *Astrophys. J.* **559**, L61.

OHSAKI, S., SHATASHVILI, N.L., YOSHIDA, Z. & MAHAJAN, S.M. 2002 Energy transformation mechanism in the solar atmosphere associated with magnetofluid coupling: explosive and eruptive events. *Astrophys. J.* **570**, 395.

SAITOH, H., YOSHIDA, Z., HIMURA, H., MORIKAWA, J. & FUKAO, M. 2004*b* Potential structure of a plasma in an internal conductor device under the influence of a biased electrode. *Phys. Plasmas* **11**, 3331–3334.

SAITOH, H., YOSHIDA, Z., HIMURA, H., MORIKAWA, J., FUKAO, M. & WAKABAYASHI, H. 2004*a* Formation of toroidal plasma flow in an internal conductor trap. *J. Plasma Fusion Res. Ser*. **6**, 179–182.

SAITOH, H., YOSHIDA, Z., NAKASHIMA, C., HIMURA, H., MORIKAWA, J. & FUKAO, M. 2004*c* Confinement of pure-electron plasmas in a toroidal magnetic-surface configuration. *Phys. Rev. Lett*. **92**, 255005.

SALINGAROS, N.A. 1990 Lorentz force and magnetic stress in force-free configurations. *Appl. Phys. Lett*. **56**, 617–619.

SHATASHVILI, N.L., MAHAJAN, S.M. & BEREZHIANI, V.I. 2016 Mechanisms for multi-scale structures in dense degenerate astrophysical plasmas. *Astrophys. Space Sci*. **361**, 70.

SHATASHVILI, N.L., MAHAJAN, S.M. & BEREZHIANI, V.I. 2019 On the relaxed states in the mixture of degenerate and non-degenerate hot plasmas of astrophysical objects. *Astrophys. Space Sci*. **364**, 148.

SHIVAMOGGI, B.K. 2011 Characteristics of plasma Beltrami states. *Eur. Phys. J.* D **64**, 393–404.

SHOHAIB, M., MASOOD, W., JAHANGIR, R., SIDDIQ, M., ALKHATEEB, S.A. & EL-TANTAWY, S.A. 2022 On the dynamics of nonlinear propagation and interaction of the modified KP solitons in multicomponent complex plasmas. *J. Ocean Engng Sci*. **7**, 555.

SOWARD, A.M. 1990 A unified approach to a class of slow dynamos. *Geophys. Astrophys. Fluid Dyn*. **53** (1–2), 81–107.

STEINHAUER, L.C. & ISHIDA, A. 1997 Relaxation of a two-specie magnetofluid. *Phys. Rev. Lett*. **79**, 3423.

STEINHAUER, L.C. & ISHIDA, A. 1998 Relaxation of a two-species magnetofluid and application to finite-flowing plasmas. *Phys. Plasmas* **5**, 2609–2622.

SUDAN, R.N. 1979 Stability of field-reversed, force-free, plasma equilibria with mass flow. *Phys. Rev. Lett*. **42**, 1277.

SUN, Q., *et al.* 2017 Formation of Field Reversed Configuration (FRC) on the Yingguang-I device. *Matter Radiat. Extremes*. **2**, 263–274.

TAYLOR, J.B. 1974 Relaxation of toroidal plasma and generation of reverse magnetic fields. *Phys. Rev. Lett*. **33**, 1139.

TAYLOR, J.B. 1986 Relaxation and magnetic reconnection in plasmas. *Rev. Mod. Phys*. **58**, 741.

VAINSHTEIN, S.I. & ROSNER, R. 1991 On turbulent diffusion of magnetic fields and the loss of magnetic flux from stars. *Astrophys. J.* **376**, 199.

VALANJU, P.M., MAHAJAN, S.M. & QUEVEDO, H.J. 2006 Equilibrium, multistability, and chiral asymmetry in rotated mirror plasmas. *Phys. Plasmas* **13**, 062105.

WAHLUND, J.E., *et al.* 1998 Observations of wave-particle interactions in the auroral ionosphere: kinetic alfvén waves and langmuir turbulence. *J. Geophys. Res.: Space Phys*. **103**, 4343.

WAHLUND, J.E., *et al.* 2009 The Mars express MARSIS sounder instrument. *Planet Space Sci*. **57**, 1975–1986.

WANG, J., CAO, J. & LIU, W. 2016 Distribution of hydrogen and oxygen ion species in the plasmasheet. *Adv. Space Res*. **58**, 84–91.

WOLTJER, L. 1958 A theorem on force-free magnetic fields. *Proc. Natl Acad. Sci. USA* **44**, 489–491.

YOSHIDA, Z., *et al.* 1998 In *Proceedings of Invited Papers, 17th IAEA Conference on Fusion Energy, Yokohama*. International Atomic Energy Agency, Vienna. IAEA-CN-69/ICP/10(R).

YOSHIDA, Z., *et al.* 1999 In *Proceedings of Invited Papers, AIP Conference on Non-Neutral Plasma Physics, New Jersey* (ed. J.J. Bollinger, R.L. Spencer & R.C. Davidson), p. 397. American Institute of Physics, CP498.

YOSHIDA, Z., *et al.* 2004 In *20th IAEA Fusion Energy Conference, Vilamoura (Portugal)*; 1–6 Nov. 2004, IC/P6–16, p. 126.

YOSHIDA, Z. & GIGA, Y. 1990 Remarks on spectra of operator rot. *Math. Z.* **204**, 235–245.

YOSHIDA, Z. & MAHAJAN, S.M. 1999 Simultaneous Beltrami conditions in coupled vortex dynamics. *J. Math. Phys*. **40**, 5080–5091.

YOSHIDA, Z. & MAHAJAN, S.M. 2002 Variational principles and self-organization in two-fluid plasmas. *Phys. Rev. Lett*. **88**, 095001.

YOSHIDA, Z., MAHAJAN, S.M., OHSAKI, S., IQBAL, M. & SHATASHVILI, N. 2001 Beltrami fields in plasmas: high-confinement mode boundary layers and high beta equilibria. *Phys. Plasmas* **8**, 2125–2131.

YOSHIDA, Z., OGAWA, Y., MORIKAWA, J., FURUKAWA, M., SAITOH, H., HIROTA, M., HORI, D., SHIRAISHI, J., WATANABE, S., NUMAZAWA, S., YANO, Y. & SUZUKI, J. 2007 Overview of Ring Trap 1 (RT-1) for exploring high-temperature magnetospheric plasma. *Trans. Fusion Sci. Technol*. **51**, 29.

https://doi.org/10.1017/S0022377824001673 Published online by Cambridge University Press